

*Chapter 1*

**NUCLEAR LIMITS ON PROPERTIES OF PULSARS AND  
GRAVITATIONAL WAVES**

*Plamen G. Krastev\**

Department of Physics and Astronomy, Texas A&M University-Commerce,  
P.O. Box 3011, Commerce, TX 75429, U.S.A.  
Department of Physics, San Diego State University,  
5500 Campanile Drive, San Diego CA 92182-1233, U.S.A.

*Bao-An Li†*

Department of Physics and Astronomy, Texas A&M University-Commerce,  
P.O. Box 3011, Commerce, TX 75429, U.S.A.

November 13, 2018

**PACS:** 04.30.-w, 97.60.Gb, 97.60.Jd, 21.65.Mn

**Keywords:** pulsars, dense matter, rapid rotation, gravitational waves

---

\*E-mail address: pkrastev@sciences.sdsu.edu

†E-mail address: Bao-An\_Li@tamu-commerce.edu

---

### Abstract

Pulsars are among the most mysterious astrophysical objects in the Universe and are believed to be rotating neutron stars formed in supernova explosions. They are unique testing grounds of dense matter theories and gravitational physics and also provide links among nuclear physics, particle physics and General Relativity. Neutron stars may exhibit some of the most extreme and exotic characteristics that could not be found elsewhere in the Universe. Their properties are largely determined by the equation of state (EOS) of neutron-rich matter, which is the chief ingredient in calculating neutron star structure and properties of related phenomena, such as gravitational wave emission from deformed pulsars. Presently, the EOS of neutron-rich matter is still very uncertain mainly due to the poorly known density dependence of the nuclear symmetry energy especially at supra-saturation densities. Nevertheless, significant progress has been made recently in constraining the density dependence of the nuclear symmetry energy mostly at sub-saturation densities using terrestrial nuclear reactions. While there are still some uncertainties especially at supra-saturation densities, these constraints could provide useful information on the limits of the global properties of pulsars and the gravitational waves to be expected from them. Here we review our recent work on constraining properties of pulsars and gravitational radiation with data from terrestrial nuclear laboratories.

## Contents

<b>1</b>	<b>Introduction</b>	<b>3</b>
<b>2</b>	<b>The equation of state of neutron-rich nuclear matter partially constrained by recent data from terrestrial heavy-ion reactions</b>	<b>5</b>
<b>3</b>	<b>Equations determining the structure of neutron stars</b>	<b>11</b>
3.1	Static stars . . . . .	12
3.2	Rotating stars . . . . .	13
<b>4</b>	<b>Constraining global properties of pulsars</b>	<b>15</b>
4.1	Keplerian (and static) sequences . . . . .	15
4.2	Rotation at various frequencies . . . . .	18
<b>5</b>	<b>Neutron star moment of inertia</b>	<b>20</b>
5.1	Slow rotation . . . . .	22
5.2	Rapid rotation . . . . .	24
5.3	Fractional moment of inertia of the neutron star crust . . . . .	26
<b>6</b>	<b>Rotation and proton fraction</b>	<b>29</b>
<b>7</b>	<b>Constraining gravitational waves from elliptically deformed pulsars</b>	<b>31</b>
7.1	Formalism relating the EOS of neutron-rich matter to the strength of gravitational waves from slowly rotating neutron stars . . . . .	32
7.2	Gravitational waves from <i>slowly</i> rotating neutron stars . . . . .	33
7.3	Gravitational waves from <i>rapidly</i> rotating neutron stars . . . . .	37

## 1 Introduction

Pulsars exhibit a large array of extreme characteristics. They are generally accepted to be rotating neutron stars – the smallest and densest stars known to exist. Matter in their cores is compressed to huge densities ranging from the density of normal nuclear matter,  $\rho_0 \approx 0.16 fm^{-3}$ , to an order of magnitude higher [1]. The number of baryons forming a neutron star is in the order of  $A \approx 10^{57}$ . Understanding properties of matter under such extreme conditions of density (and pressure) is still far from complete and represents one of the most important but also challenging problems in modern physics.

Because of their strong gravitational binding neutron stars can rotate very fast [2]. The first millisecond pulsar PSR1937+214, spinning at  $\nu = 642 Hz$  [3], was discovered in 1982, and during the next decade or so almost every year a new one was reported. In the recent years the situation changed considerably with the discovery of an anomalously large population of millisecond pulsars in globular clusters [4], where the density of stars is roughly 1000 times that in the field of the galaxy and which are therefore very favorable sites for formation of rapidly rotating neutron stars which have been spun up by the means of mass accretion from a binary companion. Presently, the number of the observed pulsars is close to 2000, and the detection rate is rather high.

In 2006 Hessels et al. [5] reported the discovery of a very rapid pulsar J1748-2446ad, rotating at  $\nu = 716 Hz$  and thus breaking the previous record (of  $642 Hz$ ). Rapid rotation could affect significantly the neutron star structure and properties, especially if the rotational frequency is near the Kepler frequency for the star. (The Kepler, or mass-shedding frequency, is the highest possible frequency an object bound by gravity can have before it starts to lose mass at the equator.) Pulsars with masses above  $1M_\odot$  enter the rapid-rotation regime, if their rotational frequencies are higher than  $1000 Hz$  [2]. Although, presently no pulsar is confirmed to rotate above the  $1000 Hz$  limit, theory does not exclude the possibility for existence of such rapidly rotating neutron stars and therefore it is important to predict their properties. (Here we should mention the recent discovery of X-ray burst oscillations from the X-ray transient XTE J1739285 [6], which could suggest that it contains an extremely rapidly rotating neutron star spinning at  $1122 Hz$ . However, this observation has not been confirmed yet.) Neutron stars are natural astrophysical laboratories of dense matter [4]. Rotating neutron stars appear as much better probes for the structure of dense baryonic matter than static ones, primarily because the particle compositions in rotating neutron stars are not frozen in, as it is the case for non-rotating neutron stars, but are varying with time [7]. The associated density changes could be as large as 60% [4] in neutron stars in binary stellar systems (e.g., low-mass X-ray binaries), which are being spun up to higher rotational frequencies, or isolated rotating neutron stars (e.g. isolated millisecond pulsars) which are spinning down to lower frequencies because of the gravitational radiation, electromagnetic dipole radiation, and a wind of electron-positron pairs [7].

Since neutron stars are objects of extremely condensed matter, the geometry of space-time is considerably altered from that of a flat space. Therefore, the construction of realistic models of neutron stars has to be done in the framework of General Relativity [1, 4]. Detailed knowledge of the equation of state (EOS) of stellar matter over a very wide range of

densities is required for solving the neutron-star structure equations. At present time the behavior of matter under extreme densities such as those found in the interiors of neutron stars is still highly uncertain and relies upon, often, rather controversial theoretical predictions. On the other hand, fortunately, heavy-ion reactions provide unique means to constrain the EOS of dense nuclear matter in terrestrial laboratories [8]. One of the major uncertainties of the EOS is the density dependence of the nuclear symmetry energy [9, 10, 11],  $E_{sym}(\rho)$ , which is the difference between the nucleon specific energies in pure neutron matter and symmetric nuclear matter. Due to its importance for the neutron star structure and many other ramifications in astrophysics and cosmology, determining the density dependence of the nuclear symmetry energy has been a major thrust of research for the intermediate energy heavy-ion community. Although extracting information about the density dependence of the nuclear symmetry energy from heavy-ion reactions is not an easy task due to the complicated roles of the isospin degree of freedom in the reaction dynamics, several promising probes of the symmetry energy have been suggested and tested in recent years [12, 13, 14, 15, 16] (see also Refs. [8, 17, 18] for reviews). In fact, some significant progress has been made in determining the  $E_{sym}(\rho)$  at subsaturation densities using: (1) isospin diffusion [19] and isoscaling [20] in heavy-ion reactions at intermediate energies [21, 22, 23, 24, 25], (2) sizes of neutron skins in heavy nuclei [10, 26, 27, 28], (3) the Pygmy dipole resonance [29] and (4) masses of nuclei [30]. At supranormal densities, a number of potential probes of the symmetry energy have been proposed [16, 31] although the available data has been very limited so far. Interestingly, circumstantial evidence for a super-soft  $E_{sym}(\rho)$  at supra-saturation densities was reported recently [32] based on the analysis of the FOPI/GSI data on pion production [33]. It is also very encouraging to notice that several dedicated experiments are being planned at several laboratories to study in more detail the symmetry energy at supra-saturation densities using high energy heavy-ion reactions induced by both stable and radioactive beams.

While global properties of spherically symmetric static neutron stars have been studied extensively and comprehensive literature exists, e.g. Refs. [9, 10, 11, 34, 35, 36, 37, 38], properties of (rapidly) rotating neutron stars have been investigated to lesser extent. Models of (rapidly) rotating neutron stars have been constructed by several research groups with various degree of approximation [4, 39, 40, 41, 42, 43, 44, 45, 46, 47, 48, 49, 50] (see Ref. [51] for a review). (Rapidly) rotating, elliptically deformed neutron stars could be one of the major candidates for emitting gravitational waves (GWs) – tiny ripples in space-time predicted by the theory of General Relativity [52]. Although GWs have not been detected directly yet, indirect evidence do exist [53]. GWs are characterized by a small dimensionless strain amplitude,  $h_0$ , which, in addition to the pulsar’s distance to detector, depends on the neutron star structure determined by the underlying EOS of stellar matter. Thus the EOS is instrumental for predicting the strength of gravitational radiation emitted from neutron stars.

The partially constrained EOS by the available terrestrial nuclear laboratory data has been used in studying several properties of neutron stars, including the mass-radius correlation [54], the surface temperature of neutron stars in connection with the changing rate of the gravitational constant  $G$  [55], the core-crust transition density [56], the frequency and damping time of the w-mode of gravitational waves [57] and the gravitational binding energy of neutron stars [58]. In this chapter we concentrate on reviewing several selected

properties of fast pulsars and the gravitational waves expected from them mostly based on our recent work reported in Refs. [59, 60, 61].

## 2 The equation of state of neutron-rich nuclear matter partially constrained by recent data from terrestrial heavy-ion reactions

In this section, we first outline the theoretical tools one uses to extract information about the EOS of neutron-rich nuclear matter from heavy-ion collisions. We put the special emphasis on exploring the density-dependence of the symmetry energy as the study on the EOS of symmetric nuclear matter with heavy-ion reactions is better known to the astrophysical community and it has been extensively reviewed, see e.g., Refs. [8, 10, 62] for recent reviews. We will then summarize the latest constraints on the density dependence of the symmetry energy at sub-saturation densities extracted from heavy-ion reactions at intermediate energies. Finally, we address the question of what kind of isospin-asymmetry, especially for dense matter, can be reached in heavy-ion reactions.

Heavy-ion reactions provide unique means to create dense nuclear matter in terrestrial laboratories similar to those found in the core of neutron stars. While unlike the matter in neutron stars the dense matter created in heavy-ion reactions is hot, accurate information about the EOS of cold matter can be extracted reliably by modeling carefully the kinetic part of the EOS during heavy-ion reactions. Depending on the beam energy, impact parameter and the reaction system, various hadrons and/or partons may be created during the reaction. To extract information about the EOS of dense matter from heavy-ion reactions requires careful modeling of the reaction dynamics and selection of sensitive observables. Among the available tools, computer simulations based on the Boltzmann-Uehling-Uhlenbeck (BUU) transport theory have been very useful, see, e.g., Refs. [8, 63] for reviews. The evolution of the phase space distribution function  $f_i(\vec{r}, \vec{p}, t)$  of nucleon  $i$  is governed by both the mean field potential  $U$  and the collision integral  $I_{collision}$  via the BUU equation

$$\frac{\partial f_i}{\partial t} + \vec{\nabla}_p U \cdot \vec{\nabla}_r f_i - \vec{\nabla}_r U \cdot \vec{\nabla}_p f_i = I_{collision}. \quad (1)$$

Normally, effects of the collision integral  $I_{collision}$  via both elastic and inelastic channels including particle productions, such as pions, are modeled via Monte Carlo sampling using either free-space experimental data or calculated in-medium cross sections for the elementary hadron-hadron scattering [63]. The collision integral is critical for modeling the kinetic part of the EOS. Information about the EOS of cold nuclear matter is obtained from the underlying mean-field potential  $U$  which is an input to the transport model. By comparing experimental data on some carefully selected observables with transport model predictions using different mean-field potentials corresponding to various EOSs, one can then constrain the corresponding EOS. The specific constraints on the density dependence of the nuclear symmetry energy that we are using in this work were obtained by analyzing the isospin diffusion data [19] within the IBUU04 version of an isospin and momentum dependent transport model [64]. In this model, an isospin and momentum-dependent interaction (MDI) [65] is used. With this interaction, the potential energy density  $V(\rho, T, \delta)$  at total

density  $\rho$ , temperature  $T$  and isospin asymmetry  $\delta$  is

$$\begin{aligned}
V(\rho, T, \delta) &= \frac{A_u \rho_n \rho_p}{\rho_0} + \frac{A_l}{2\rho_0} (\rho_n^2 + \rho_p^2) + \frac{B}{\sigma + 1} \frac{\rho^{\sigma+1}}{\rho_0^\sigma} (1 - x\delta^2) \\
&+ \sum_{\tau, \tau'} \frac{C_{\tau, \tau'}}{\rho_0} \int \int d^3 p d^3 p' \frac{f_\tau(\vec{r}, \vec{p}) f_{\tau'}(\vec{r}, \vec{p}')}{1 + (\vec{p} - \vec{p}')^2 / \Lambda^2}
\end{aligned} \tag{2}$$

In the mean field approximation, Eq. (2) leads to the following single particle potential for a nucleon with momentum  $\vec{p}$  and isospin  $\tau$

$$\begin{aligned}
U_\tau(\rho, T, \delta, \vec{p}, x) &= A_u(x) \frac{\rho_{-\tau}}{\rho_0} + A_l(x) \frac{\rho_\tau}{\rho_0} + B \left( \frac{\rho}{\rho_0} \right)^\sigma (1 - x\delta^2) \\
&- 8\tau x \frac{B}{\sigma + 1} \frac{\rho^{\sigma-1}}{\rho_0^\sigma} \delta \rho_{-\tau} + \sum_{t=\tau, -\tau} \frac{2C_{\tau, t}}{\rho_0} \int d^3 \vec{p}' \frac{f_t(\vec{r}, \vec{p}')}{1 + (\vec{p} - \vec{p}')^2 / \Lambda^2},
\end{aligned} \tag{3}$$

where  $\tau = 1/2$  ( $-1/2$ ) for neutrons (protons),  $x$ ,  $A_u(x)$ ,  $A_l(x)$ ,  $B$ ,  $C_{\tau, \tau}$ ,  $C_{\tau, -\tau}$ ,  $\sigma$ , and  $\Lambda$  are all parameters given in Ref. [65]. The last two terms in Eq. (3) contain the momentum dependence of the single-particle potential, including that of the symmetry potential if one allows for different interaction strength parameters  $C_{\tau, -\tau}$  and  $C_{\tau, \tau}$  for a nucleon of isospin  $\tau$  interacting, respectively, with unlike and like nucleons in the background fields. It is worth mentioning that the nucleon isoscalar potential estimated from  $U_{isoscalar} \approx (U_n + U_p)/2$  agrees with the prediction of variational many-body calculations for symmetric nuclear matter [66] in a broad density and momentum range [64]. Moreover, the EOS of symmetric nuclear matter for this interaction is consistent with that extracted from the available data on collective flow and particle production in relativistic heavy-ion collisions up to five times the normal nuclear matter [8]. On the other hand, the corresponding isovector (symmetry) potential can be estimated from  $U_{sym} \approx (U_n - U_p)/2\delta$ . At normal nuclear matter density, the MDI symmetry potential agrees very well with the Lane potential extracted from nucleon-nucleus and (n,p) charge exchange reactions available for nucleon kinetic energies up to about 100 MeV [64]. At abnormal densities and higher nucleon energies, however, there is no experimental constrain on the symmetry potential available at present.

The different  $x$  values in the MDI interaction are introduced to vary the density dependence of the nuclear symmetry energy while keeping other properties of the nuclear equation of state fixed. Specifically, choosing the incompressibility  $K_0$  of cold symmetric nuclear matter at saturation density  $\rho_0$  to be 211 MeV leads to the dependence of the parameters  $A_u$  and  $A_l$  on the  $x$  parameter according to

$$A_u(x) = -95.98 - x \frac{2B}{\sigma + 1}, \quad A_l(x) = -120.57 + x \frac{2B}{\sigma + 1}, \tag{4}$$

with  $B = 106.35$  MeV.

With the potential contribution from Eq. (2) and the well-known contribution from nucleon kinetic energies in the Fermi gas model, the EOS and the symmetry energy at zero temperature can be easily obtained. As shown in Fig. (1), varying the parameter  $x$  leads to a broad range of the density dependence of the nuclear symmetry energy, similar to those

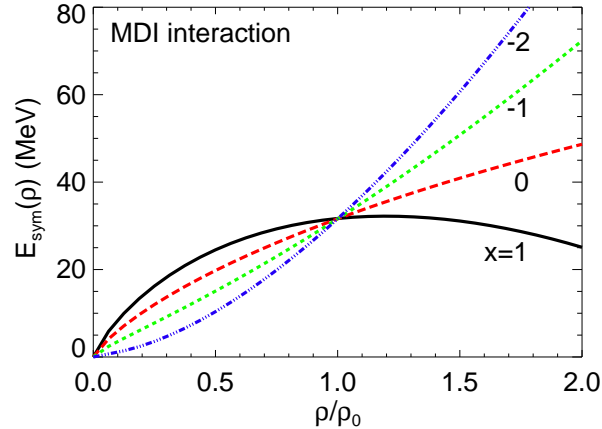


Figure 1: The density dependence of the nuclear symmetry energy for different values of the parameter  $x$  in the MDI interaction. Taken from [72].

predicted by various microscopic and/or phenomenological many-body theories. As previously demonstrated in [24] and [54], only equations of state with  $x$  between  $-1$  and  $0$  have symmetry energies in the sub-saturation density region consistent with the isospin diffusion data and the available measurements of the skin thickness of  $^{208}\text{Pb}$  using hadronic probes. More recently however, it was shown that at supra-saturation densities the symmetry energy could be much softer than the extrapolation of the symmetry energy with  $x = 0$  [32]. The possibility for a super-soft symmetry energy at supra-saturation densities could have important consequences for the neutron star stability and the nature of gravity at sub-millimeter distances [67]. Nevertheless, as the first and a conservative step in our studies of the properties of (rotating) neutron stars [59, 60] and the gravitational waves expected from them [61], we have used  $x = -1$  and  $x = 0$  to compute the range of possible (rotating) neutron star configurations. The  $E_{sym}(\rho)$  with  $x = 0$  is also consistent with the RMF prediction using the FSUGold interaction [68]. In this review, we thus consider only the two limiting cases with  $x = 0$  and  $x = -1$  as boundaries of the symmetry energy consistent with the available terrestrial nuclear laboratory data at sub-saturation densities.

To facilitate comparisons with other models in the literature, it is useful to parameterize the  $E_{sym}(\rho)$  from the MDI interaction and list its characteristics. Within phenomenological models it is customary to separate the symmetry energy into the kinetic and potential parts,

Table 1: The parameters  $F$  (MeV),  $G$ ,  $K_{sym}$  (MeV),  $L$  (MeV), and  $K_{asy}$  (MeV) for different values of  $x$ . Taken from [22].

$x$	$F$	$G$	$K_{sym}$	$L$	$K_{asy}$
1	107.232	1.246	-270.4	16.4	-368.8
0	129.981	1.059	-88.6	62.1	-461.2
-1	3.673	1.569	94.1	107.4	-550.3
-2	-38.395	1.416	276.3	153.0	-641.7

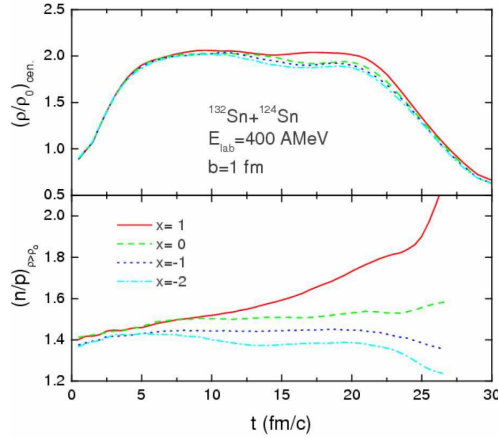


Figure 2: Central baryon density (upper panel) and isospin asymmetry (lower panel) of high density region in the reaction of  $^{132}\text{Sn} + ^{124}\text{Sn}$  at a beam energy of 400 MeV/nucleon and an impact parameter of 1 fm. Taken from Ref. [72].

see, e.g. [69],

$$E_{sym}(\rho) = (2^{2/3} - 1) \frac{3}{5} E_F^0(\rho/\rho_0)^{2/3} + E_{sym}^{\text{pot}}(\rho). \quad (5)$$

With the MDI interaction, the potential part of the nuclear symmetry energy can be well parameterized by

$$E_{sym}^{\text{pot}}(\rho) = F(x)\rho/\rho_0 + (18.6 - F(x))(\rho/\rho_0)^{G(x)}, \quad (6)$$

with  $F(x)$  and  $G(x)$  given in Table 1 for  $x = 1, 0, -1$  and  $-2$ . The MDI parameterizations for the  $E_{sym}^{\text{pot}}(\rho)$  are similar to but significantly different from those used in Ref. [69]. Also shown in Table 1 are other characteristics of the symmetry energy, including its slope parameter  $L$  and curvature parameter  $K_{sym}$  at  $\rho_0$ , as well as the isospin-dependent part  $K_{asy}$  of the isobaric incompressibility of asymmetric nuclear matter [22]. The symmetry energy in the subsaturation density region with  $x=0$  and  $-1$  can be roughly approximately by  $E_{sym}(\rho) \approx 31.6(\rho/\rho_0)^{0.69}$  and  $E_{sym}(\rho) \approx 31.6(\rho/\rho_0)^{1.05}$ , respectively.

What is the maximum isospin asymmetry reached, especially in the supra-normal density regions, in typical heavy-ion reactions? How does it depend on the symmetry energy? Do both the density and isospin asymmetry reached have to be high simultaneously in order to probe the symmetry energy at supra-normal densities with heavy-ion reactions? The answers to these questions are important for us to better understand the advantages and limitations of using heavy-ion reactions to probe the EOS of neutron-rich nuclear matter and properly evaluate their impacts on astrophysics.

To answer these questions we first show in Fig. 2 the central baryon density (upper window) and the average  $(n/p)_{\rho \geq \rho_0}$  ratio (lower window) of all regions with baryon densities higher than  $\rho_0$  in the reaction of  $^{132}\text{Sn} + ^{124}\text{Sn}$  at a beam energy of 400 MeV/nucleon and an impact parameter of 1 fm. It is seen that the maximum baryon density is about 2 times the normal nuclear matter density. Moreover, the compression is rather insensitive to the symmetry energy because the latter is relatively small compared to the EOS of symmetric



nuclear matter around this density. The high density phase lasts for about 15 fm/c from 5 to 20 fm/c for this reaction. It is interesting to see in the lower window that the isospin asymmetry of the high density region is quite sensitive to the density dependence of the symmetry energy used in the calculation. The soft (e.g.,  $x = 1$ ) symmetry energy leads to a significantly higher value of  $(n/p)_{\rho \geq \rho_0}$  than the stiff one (e.g.,  $x = -2$ ). This is consistent with the well-known isospin fractionation phenomenon in asymmetric nuclear matter [70, 71]. Because of the  $E_{sym}(\rho)\delta^2$  term in the EOS of asymmetric nuclear matter, it is energetically more favorable to have a higher isospin asymmetry  $\delta$  in the high density region with a softer symmetry energy functional  $E_{sym}(\rho)$ . In the supra-normal density region, as shown in Fig. 1, the symmetry energy changes from being soft to stiff when the parameter  $x$  varies from 1 to -2. Thus the value of  $(n/p)_{\rho \geq \rho_0}$  becomes lower as the parameter  $x$  changes from 1 to -2. It is worth mentioning that the initial value of the quantity  $(n/p)_{\rho \geq \rho_0}$  is about 1.4 which is less than the average n/p ratio of 1.56 of the reaction system. This is because of the neutron-skins of the colliding nuclei, especially that of the projectile  $^{132}\text{Sn}$ . In the neutron-rich nuclei, the n/p ratio on the low-density surface is much higher than that in their interior. Also because of the  $E_{sym}(\rho)\delta^2$  term in the EOS, the isospin-asymmetry in the low density region is much lower than the supra-normal density region as long as the symmetry increases with density. In fact, as shown in Fig. 2 of Ref. [54], the isospin-asymmetry of the low density region can become much higher than the isospin asymmetry of the reaction system.

It is clearly seen that the dense region can become either neutron-richer or neutron-poorer with respect to the initial state depending on the symmetry energy functional  $E_{sym}(\rho)$  used. As long as the symmetry energy increases with the increasing density, the isospin asymmetry of the supra-normal density region is always lower than the isospin asymmetry of the reaction system. Thus, even with radioactive beams, the supra-normal density region can not be both dense and neutron-rich simultaneously, unlike the situation in the core of neutron stars, unless the symmetry energy starts decreasing at high densities. The high density behavior of the symmetry energy is probably among the most uncertain properties of dense matter as stressed by [73, 74]. Indeed, some predictions show that the symmetry energy can decrease with increasing density above certain density and may even finally become negative. This extreme behavior was first predicted by some microscopic many-body theories, see e.g., Refs. [11, 75, 76]. It has also been shown that the symmetry energy can become negative at various high densities within the Hartree-Fock approach using the original Gogny force [77], the density-dependent M3Y interaction [78, 79] and about 2/3 of the 87 Skyrme interactions that have been widely used in the literature [80]. The mechanism leading to and physical meaning of a negative symmetry energy are the topics of some very recent studies [81]. It was found that the spin-isospin dependence of the three-body force and the in-medium properties of the short-range tensor force due to the  $\rho$ -meson exchange are the main sources of the very uncertain high-density behavior of the nuclear symmetry energy.

The isospin effects in heavy-ion reactions are determined mainly by the  $E_{sym}(\rho)\delta^2$  term in the EOS. One expects a larger effect if the isospin-asymmetry is higher. Thus, ideally, one would like to have situations where both the density and isospin asymmetry are sufficiently high simultaneously as in the cores of neutron stars in order to observe the strongest effects due to the symmetry energy at supra-normal densities. However, since it

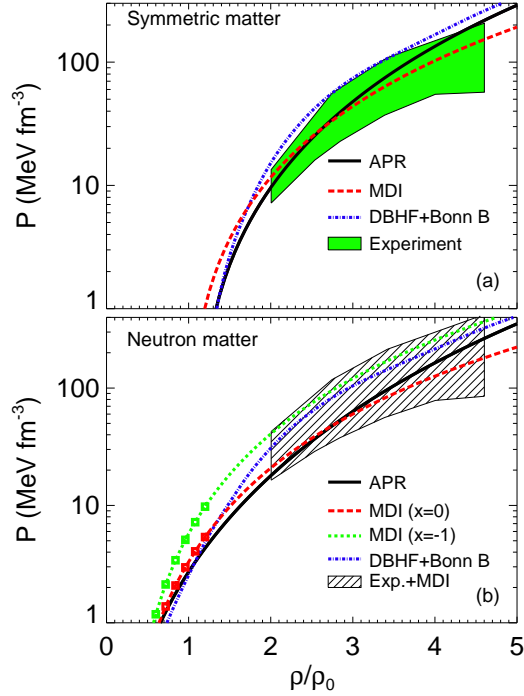


Figure 3: (Color online) Pressure as a function of density for symmetric (upper panel) and pure neutron (lower panel) matter. The green area in the upper panel is the experimental constraint on symmetric matter extracted by Danielewicz, Lacey and Lynch [8] from analyzing the collective flow in relativistic heavy-ion collisions. The corresponding constraint on the pressure of pure neutron matter, obtained by combining the flow data and an extrapolation of the symmetry energy functionals constrained below  $1.2\rho_0$  ( $\rho_0 = 0.16\text{fm}^{-3}$ ) by the isospin diffusion data, is the shaded black area in the lower panel. Results are taken partially from Ref. [8].

is the product of the symmetry energy and the isospin-asymmetry that matters, one can still probe the symmetry energy at high densities where the isospin asymmetry is generally low with symmetry energy functionals that increase with density. Therefore, even if the high density region may not be as neutron-rich as in neutron stars, heavy-ion collisions can still be used to probe the symmetry energy at high densities useful for studying properties of neutron stars.

For many astrophysical studies (as those in this chapter), it is more convenient to express the EOS in terms of the pressure as a function of density and isospin asymmetry. In Fig. 3 we show pressure as a function of density for two extreme cases: symmetric (upper panel) and pure neutron matter (lower panel). The green area in the density range of  $\rho_0 = [2.0 - 4.6]$  is the experimental constraint on the pressure  $P_0$  of symmetric nuclear matter extracted by Danielewicz, Lacey and Lynch from analyzing the collective flow data from relativistic heavy-ion collisions [8]. The pressure of pure neutron matter  $P_{PNM} = P_0 + \rho^2 dE_{sym}(\rho)/d\rho$  depends on the density behavior of the nuclear symmetry

Table 2: Saturation properties of the nuclear EOSs (for symmetric nuclear matter) shown in Fig. 3.

EOS	$\rho_0$ ( $fm^{-3}$ )	$E_s$ ( $MeV$ )	$\kappa$ ( $MeV$ )	$m^*(\rho_0)$ ( $MeV/c^2$ )	$E_{sym}(\rho_0)$ ( $MeV$ )
MDI	0.160	-16.08	211.00	629.08	31.62
APR	0.160	-16.00	266.00	657.25	32.60
DBHF+Bonn B	0.185	-16.14	259.04	610.30	33.71

The first column identifies the equation of state. The remaining columns exhibit the following quantities at the nuclear saturation density: saturation (baryon) density; energy-per-particle; compression modulus; nucleon effective mass; symmetry energy.

energy  $E_{sym}(\rho)$ . Since the experimental constraints on the symmetry energy from terrestrial laboratory experiments are available mostly for densities less than about  $1.2\rho_0$  as indicated by the green and red squares in the lower panel, which is in contrast to the constraint on the symmetric EOS that is only available at much higher densities, the most reliable estimate of the EOS of neutron-rich matter can thus be obtained by extrapolating the underlying model EOS for symmetric matter and the symmetry energy in their respective density ranges to all densities. Shown by the shaded black area in the lower panel is the resulting best estimate of the pressure of high density pure neutron matter based on the predictions from the MDI interaction with  $x = 0$  and  $x = -1$  as the lower and upper bounds on the symmetry energy and the flow-constrained symmetric EOS. As one expects and consistent with the estimate in Ref. [8], the estimated error bars of the high density pure neutron matter EOS are much wider than the uncertainty range of the symmetric EOS. For the four interactions indicated in the figure, their predicted EOSs cannot be distinguished by the estimated constraint on the high density pure neutron matter. In addition to the MDI EOS, in Fig. 3 we show results by Akmal et al. [82] with the  $A18 + \delta v + UIX^*$  interaction (APR) and recent Dirac-Brueckner-Hartree-Fock (DBHF) calculations [83] with Bonn B One-Boson-Exchange (OBE) potential (DBHF+Bonn B) [85]. (Older calculations of the DBHF+Bonn B EOS can be found in Refs. [84, 11].) The saturation properties of the nuclear equations of state applied in this work are summarized in Table 2.

### 3 Equations determining the structure of neutron stars

For completeness, in the following we briefly recall the equations determining the structure of both static and (rapidly) rotating neutron stars based on the well-established formalism in the astrophysical literature. As already mentioned in the introduction, neutron stars are objects of extremely compressed matter and therefore proper understanding of their properties requires application of both General Relativity and the theories of dense matter. In this respect, neutron stars provide a direct link between two of the frontiers of modern physics - General Relativity and strong interactions in dense matter [4]. The connection between

both branches of physics is provided by Einstein's field equations

$$G^{\mu\nu} = R^{\mu\nu} - \frac{1}{2}g^{\mu\nu}R = 8\pi T^{\mu\nu}(\epsilon, P(\epsilon)), \quad (7)$$

( $\mu, \nu = 0, 1, 2, 3$ ) which couple the Einstein curvature tensor,  $G^{\mu\nu}$ , to the energy-momentum tensor,

$$T^{\mu\nu} = (\epsilon + P)u^\mu u^\nu + Pg^{\mu\nu}, \quad (8)$$

of stellar matter. In the above equations  $P$  and  $\epsilon$  denote pressure and mass energy density, while  $R^{\mu\nu}$ ,  $g^{\mu\nu}$ , and  $R$  denote the Ricci tensor, the metric tensor, and the Ricci scalar curvature respectively (see e.g., [1]). In Eq. (8)  $u^\mu$  is the unit time-like four-velocity satisfying  $u^\mu u_\mu = -1$ . The tensor  $T^{\mu\nu}$  contains the EOS of stellar matter in the form  $P(\epsilon)$ . In general, Einstein's field equations and those of the nuclear many-body problem were to be solved simultaneously since the baryons and quarks follow the geodesics of the curved space-time whose geometry, determined by the Einstein's field equations, is coupled to the total mass energy density of matter [4]. In the case of neutron stars, as for all astrophysical situations for which the long-range gravitational force can be separated from the short-range strong force, the deviation from flat space-time at the length-scale of the strong interactions ( $\sim 1fm$ ) is practically zero up to the highest densities achieved in the neutron star interiors. (This is not to be confused with the global length-scale of neutron stars ( $\sim 10km$ ) for which  $M/R \sim 0.3$  depending on the star's mass (in units  $c = G = 1$  so that  $M_\odot \approx 1.475km$ .) In other words, gravity curves space-time only on a macroscopic scale but to a very good approximation leaves it flat on a microscopic scale. To achieve an appreciable curvature on a microscopic level at which the strong interactions dominate the particle dynamics mass densities greater than  $\sim 10^{40}g\text{ cm}^{-3}$  would be necessary [4, 86]. Under this circumstances the problem of constructing models of neutron stars separates into two distinct tasks. First, the short-range effects of the nuclear forces are described by the principles of many-body nuclear physics in a local inertial frame (co-moving proper reference frame) in which space-time is flat. Second, the coupling between the long-range gravitational force and matter is accounted for by solving the general relativistic equations for the gravitational field described by the curvature of space-time, leading to the global structure of stellar configurations.

### 3.1 Static stars

In the case of spherically symmetric static (non-rotating) stars the metric has the famous Schwarzschild form:

$$ds^2 = -e^{2\phi(r)} dt^2 + e^{2\Lambda(r)} dr^2 + r^2(d\theta^2 + \sin^2\theta d\phi^2), \quad (9)$$

( $c = G = 1$ ) where the metric functions  $\phi(r)$  and  $\Lambda(r)$  are given by:

$$e^{2\Lambda(r)} = (1 - \gamma(r))^{-1}, \quad (10)$$

$$e^{2\phi(r)} = e^{-2\Lambda(r)} = (1 - \gamma(r)) \quad r > R_{star}, \quad (11)$$

with

$$\gamma(r) = \begin{cases} \frac{2m(r)}{r} & \text{if } r < R_{star} \\ \frac{2M}{r} & \text{if } r > R_{star} \end{cases} \quad (12)$$

For a static star Einstein's field equations (Eq. (7)) reduce then to the familiar Tolman-Oppenheimer-Volkoff equation (TOV) [87, 88]:

$$\frac{dP(r)}{dr} = -\frac{\epsilon(r)m(r)}{r^2} \left[ 1 + \frac{P(r)}{\epsilon(r)} \right] \left[ 1 + \frac{4\pi r^3 p(r)}{m(r)} \right] \left[ 1 - \frac{2m(r)}{r} \right]^{-1} \quad (13)$$

where the gravitational mass within a sphere of radius  $r$  is determined by

$$\frac{dm(r)}{dr} = 4\pi\epsilon(r)r^2 \quad (14)$$

The metric function  $\phi(r)$  is determined through the following differential equation:

$$\frac{d\phi(r)}{dr} = -\frac{1}{\epsilon(r) + P(r)} \frac{dP(r)}{dr}, \quad (15)$$

with the boundary condition at  $r = R$

$$\phi(r = R) = \frac{1}{2} \ln \left( 1 - \frac{2M}{R} \right) \quad (16)$$

To proceed to the solution of these equations, it is necessary to provide the EOS of stellar matter in the form  $P(\epsilon)$ . Starting from some central energy density  $\epsilon_c = \epsilon(0)$  at the center of the star ( $r = 0$ ), and with the initial condition  $m(0) = 0$ , the above equations can be integrated outward until the pressure vanishes, signifying that the stellar edge is reached. Some care should be taken at  $r = 0$  since, as seen above, the TOV equation is singular there. The point  $r = R$  where the pressure vanishes defines the radius of the star and  $M = m(R) = 4\pi \int_0^R \epsilon(r')r'^2 dr'$  its gravitational mass.

For a given EOS, there is a unique relationship between the stellar mass and the central density  $\epsilon_c$ . Thus, for a particular EOS, there is a unique sequence of stars parameterized by the central density (or equivalently the central pressure  $P(0)$ ).

### 3.2 Rotating stars

Equations of stellar structure of (rapidly) rotating neutron stars are considerably more complex than those of spherically symmetric stars [4]. These complications arise due to the rotational deformations in rotating stars (i.e., flattening at the poles and bulging at the equator), which lead to a dependence of the star's metric on the polar coordinate  $\theta$ . In addition, rotation stabilizes the star against gravitational collapse and therefore rotating neutron stars are more massive than static ones. A larger mass, however, causes greater curvature of space-time. This renders the metric functions frequency-dependent. Finally, the general relativistic effect of dragging the local inertial frames implies the occurrence of an additional non-diagonal term,  $g^{t\phi}$ , in the metric tensor  $g^{\mu\nu}$ . This term imposes a self-consistency condition on the stellar structure equations, since the degree at which the local inertial frames

are dragged along by the star, is determined by the initially unknown stellar properties like mass and rotational frequency [4].

The structure equations of rapidly rotating neutron stars have been computed with the *RNS*<sup>1</sup> code developed and made available to the public by Nikolaos Stergioulas [46]. Here we outline briefly the equations solved by the *RNS* code. The coordinates of the stationary, axial symmetric space-time used to model a (rapidly) rotating neutron star are defined through a generalization of Bardeen's metric [51]:

$$ds^2 = -e^{\gamma+\rho} dt^2 + e^{2\alpha} (dr^2 + r^2 d\theta^2) + e^{\gamma-\rho} r^2 \sin^2 \theta (d\phi - \omega dt^2), \quad (17)$$

where the metric potentials  $\gamma$ ,  $\rho$ ,  $\alpha$ , and the angular velocity of the stellar fluid relative to the local inertial frame,  $\omega$ , are functions of the quasi-isotropic radial coordinates,  $r$ , and the polar angle  $\theta$  only. The matter inside a rigidly rotating star is approximated as a perfect fluid [51], whose energy momentum tensor is given by Eq. (8). The proper velocity of matter,  $v$ , relative to the local Zero Angular Momentum Observer (ZAMO) [89] is defined as

$$v = r \sin(\theta) (\Omega - \omega) e^{-\rho(r)} \quad (18)$$

with  $\Omega = u^3/u^0$  the angular velocity of a fluid element. The four-velocity is given by

$$u^\mu = \frac{e^{-(\gamma+\rho)/2}}{\sqrt{(1-v^2)}} (1, 0, 0, \Omega) \quad (19)$$

In the above equation the function  $(\gamma + \rho)/2$  represents the relativistic generalization of the Newtonian gravitational potential, while  $\exp[(\gamma + \rho)/2]$  is a time dilation factor between an observer moving with angular velocity  $\omega$  and one at infinity. Substitution of Eq. (19) into Einstein's fields equations projected onto the ZAMO reference frame gives three elliptic partial differential equations for the metric potentials  $\gamma$ ,  $\rho$ , and  $\omega$ , and two linear ordinary differential equations for the metric potential  $\alpha$ . Technically, the elliptic differential equations for the metric functions are converted into integral equations which are then solved iteratively applying Green's function approach [44, 51].

From the relativistic equations of motion, the equations of hydrostatic equilibrium for a barotropic fluid may be obtained as [51, 89]:

$$h(P) - h_p = \frac{1}{2} [\omega_p + \rho_p - \gamma - \rho - \ln(1 - v^2) + A^2(\omega - \Omega_c)^2], \quad (20)$$

with  $h(P)$  the specific enthalpy,  $P_p$  the re-scaled pressure,  $h_p$  the specific enthalpy at the pole,  $\gamma_p$  and  $\rho_p$  the values of the metric potentials at the pole,  $\Omega_c = r_e \Omega$ , and  $A$  a rotational constant [51]. The subscripts  $p$ ,  $e$ , and  $c$  label the corresponding quantities at the pole, equator and center respectively. The *RNS* code solves iteratively the integral equations for  $\rho$ ,  $\gamma$  and  $\omega$ , and the ordinary differential equation for the metric function  $\alpha$  coupled with Eq. (20) and the equations for hydrostatic equilibrium at the stellar center and equator (given  $h(P_c)$  and  $h(P_e) = 0$ ) to obtain  $\rho$ ,  $\gamma$ ,  $\alpha$ ,  $\omega$ , the equatorial coordinate radius  $r_e$ , angular velocity  $\Omega$ , energy density  $\epsilon$ , and pressure  $P$  throughout the star.

<sup>1</sup>Thanks to Nikolaos Stergioulas the *RNS* code is available as a public domain program at <http://www.gravity.phys.uwm.edu/rns/>

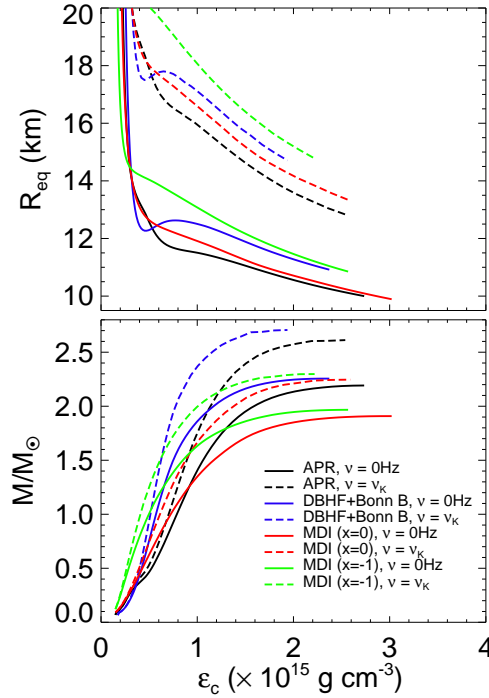


Figure 4: (Color online) Neutron star masses and radii. Neutron star equatorial radii (upper panel) and total gravitational mass (lower panel) versus central energy density  $\epsilon_c$ . Both static (solid lines) and Keplerian (broken lines) models are shown. Taken from Ref. [59].

## 4 Constraining global properties of pulsars

We construct one-parameter 2-D stationary configurations of (rapidly) rotating neutron stars employing several nucleonic EOSs and the *RNS* code. We assume a simple model of stellar matter of nucleons and light leptons (electrons and muons) in beta-equilibrium. Below the baryon density of approximately  $0.07 fm^{-3}$  the equations of state applied here are supplemented by a crustal EOS, which is more suitable for the low density regime. Namely, we apply the EOS by Pethick et al. [90] for the inner crust and the one by Haensel and Pichon [91] for the outer crust. In the core we assume a continuous functional for the EOSs employed in this work. (See Ref. [11] for a detailed description of the extrapolation procedure for the DBHF+Bonn B EOS.)

### 4.1 Keplerian (and static) sequences

In what follows we examine the effect of ultra-fast rotation at the Kepler frequency on the neutron star gravitational masses and radii. The equilibrium configurations for both static and (rapidly) rotating neutron stars are parameterized in terms of the central mass energy density,  $\epsilon_c = \epsilon(0)$  (or equivalently central pressure,  $P_c = P(0)$ ). This functional dependence is shown in Fig. 4, where we display the stellar *equatorial* radius (upper frame) and total gravitational mass (lower frame) versus central energy density for the EOSs applied in

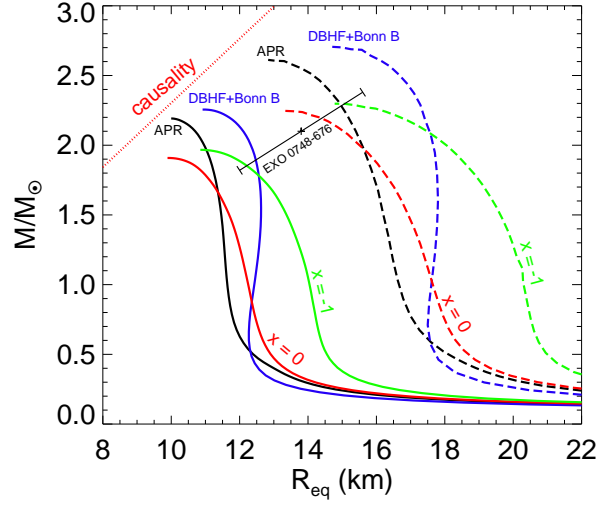


Figure 5: (Color online) Mass-radius relation. Both static (solid lines) and Keplerian (broken lines) sequences are shown. The  $1 - \sigma$  error bar corresponds to the measurement of the mass and radius of EXO 0748-676 [95]. Taken from Ref. [59].

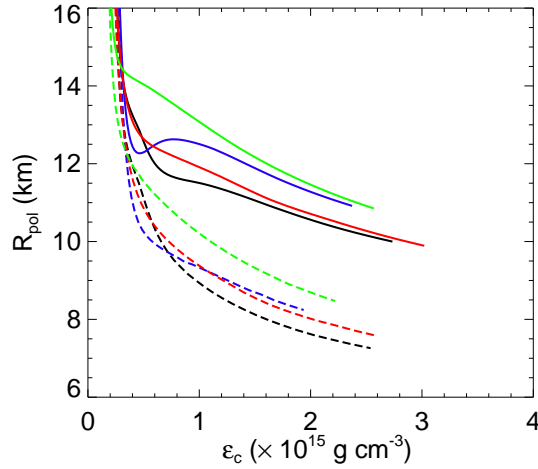


Figure 6: (Color online) Neutron-star polar radius versus central energy density. Both static (solid lines) and Keplerian (broken lines) sequences are shown. The labeling of the curves is the same as in Fig. 4. Taken from Ref. [59].

this work. Predictions for both static and maximally rotating models are shown. The main feature of the mass-density plot is that there exists a maximum value of the gravitational mass of a neutron star that a given EOS can support [4]. This holds for both static and (rapidly) rotating stars. The sequences shown in Fig. 4 terminate at the "maximum mass" point. Comparing the results for static and rotating stars, it is seen clearly that the rapid rotation increases noticeably the mass that can be supported against collapse while lowering the central density of the maximum-mass configuration. This is what one should expect, since, as already mentioned, rotation stabilizes the star against the gravitational pull providing an



Table 3: Maximum-mass static (non-rotating) models.

EOS	$M_{max}(M_{\odot})$	$R(km)$	$\epsilon_c(\times 10^{15} g cm^{-3})$
MDI( $\chi=0$ )	1.91	9.89	3.02
APR	2.19	9.98	2.73
MDI( $\chi=-1$ )	1.97	10.85	2.57
DBHF+Bonn B	2.26	10.91	2.37

The first column identifies the equation of state. The remaining columns exhibit the following quantities for the static models with maximum gravitational mass: gravitational mass; radius; central mass energy density.

Table 4: Maximum-mass rapidly rotating models at the Kepler frequency  $\nu = \nu_k$ .

EOS	$M_{max}(M_{\odot})$	Increase (%)	$\epsilon_c(\times 10^{15} g cm^{-3})$	$\nu_k(Hz)$	$\nu_k^{FIP}(Hz)$
MDI( $\chi=0$ )	2.25	15	2.59	1742	1610
APR	2.61	17	2.53	1963	1699
MDI( $\chi=-1$ )	2.30	14	2.21	1512	1423
DBHF+Bonn B	2.71	17	1.94	1644	1510

The first column identifies the equation of state. The remaining columns exhibit the following quantities for the maximally rotating models with maximum gravitational mass: gravitational mass; its percentage increase over the maximum gravitational mass of static models; central mass energy density; maximum rotational frequency; Kepler frequency as computed via the empirical relation given by Eq. (21) [93].

extra (centrifugal) repulsion. The rotational effect on the mass-radius relation is illustrated in Fig. 5 where the gravitational mass is given as a function of the circumferential radius. For rapid rotation at the Kepler frequency, a mass increase up to  $\sim 17\%$  (Table 4) is obtained, depending on the EOS. The equatorial radius increases by several kilometers, while the polar radius decreases by several kilometers (see Fig. 6) leading to an overall oblate shape of the rotating star. Table 3 summarizes the properties (masses, radii and central energy densities) of the maximum-mass non-rotating neutron star configurations. Our studies on the effect of rapid rotation on the upper mass limits for the four EOSs considered in this chapter are presented in Table 4. In each case the upper mass limit is obtained for a model at the mass-shedding limit where  $\nu = \nu_k$ , with central density  $\sim 15\%$  below that of the static model with the largest mass. These findings are consistent with those in Refs. [92] and [46]. Table 4 also provides an estimate of the upper limiting rotation rate of a neutron star. In general, softer EOSs permit larger rotational frequencies since the resulting stellar models are more centrally condensed, see e.g., Ref. [92]. In the last column of Table 4 we show the Kepler frequencies computed via the empirical relation

$$\frac{\Omega_k}{10^4 s^{-1}} = 0.72 \left( \frac{M_s}{M_{\odot}} \right)^{1/2} \left( \frac{R_s}{10 km} \right)^{-3/2} \quad (21)$$

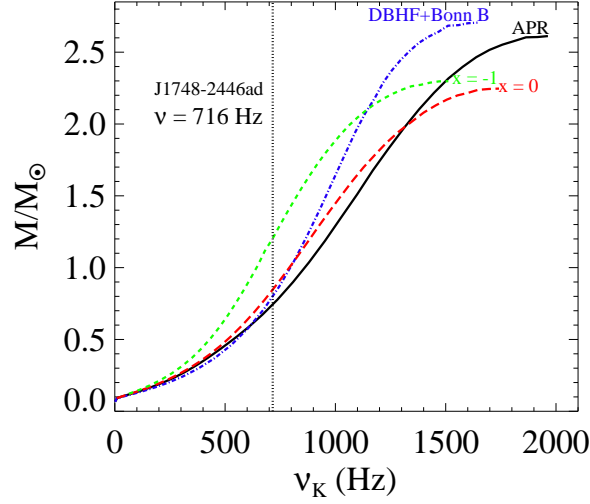


Figure 7: (Color online) Mass versus Keplerian (mass-shedding) frequency  $\nu_k$ . Adapted from Ref. [59].

proposed in Ref. [93]. The uncertainty of Eq. (21) is  $\sim 10\%$  (see Ref. [94] for an improved version of the empirical formula). At the time of constructing the above relation Friedman et al. [93] did not consider a then unknown class of minimum period EOSs [96] which explains why the numbers in the last column of Table 4 exhibit larger deviation from the exact numerical solutions (in column five). This is particularly pronounced for the APR EOS for which the approximated Kepler frequency deviates  $\sim 14\%$  from the exact solution. (Note that the APR EOS has the lowest period among the EOSs considered here.)

Fig. 7 displays the neutron star gravitational mass as a function of the Kepler frequency,  $\nu_k$ . The vertical dotted line corresponds to the frequency of the fastest neutron star presently known (J1748-2446ad [5]). The figure suggests that the higher the rotational frequency, the larger the mass for the possible stable neutron star configurations. We discuss this further in the next subsection.

## 4.2 Rotation at various frequencies

In this subsection we study neutron stars rotating at various (fixed) frequencies. Stability with respect to the mass-shedding from equator implies that at a given gravitational mass the equatorial radius  $R_{eq}$  should be smaller than  $R_{eq}^{max}$  corresponding to the Keplerian limit [2]. The value of  $R_{eq}^{max}$  results from the condition that the frequency of a test particle at circular equatorial orbit of radius  $R_{eq}^{max}$  just above the equator of the actual rotating star is equal to the rotational frequency of the star. As reported by Bejger et al. [2] the relation between  $M$  and  $R_{eq}$  at the “mass-shedding point” is very well approximated by the expression for the orbital frequency for a test particle orbiting at  $r = R_{eq}$  in the Schwarzschild space-time created by a spherical mass. The formula satisfying  $\nu_{orb}^{Schw.} = \nu$ , represented by the dotted line in Figs. 8, 9 and 10 is given by

$$\frac{1}{2\pi} \left( \frac{GM}{R_{eq}^3} \right) = \nu, \quad (22)$$

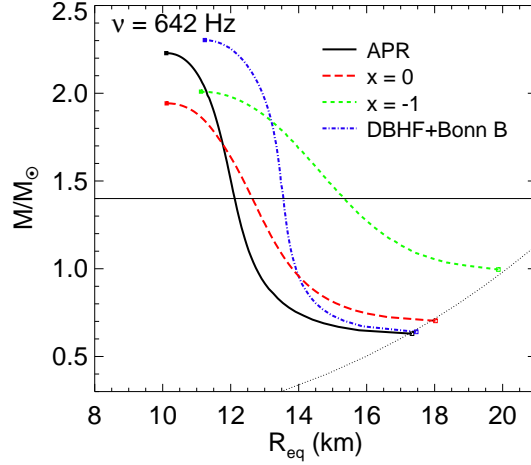


Figure 8: (Color online) Gravitational mass versus circumferential radius for neutron stars rotating at  $\nu = 642Hz$ . See text for details.

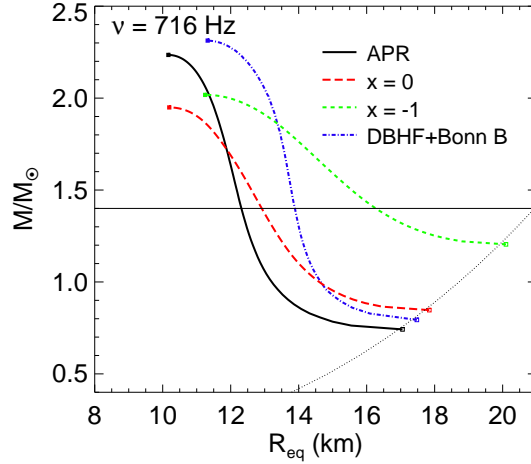


Figure 9: (Color online) Gravitational mass versus circumferential radius for neutron stars rotating at  $\nu = 716Hz$ .

where  $\nu = 642Hz$  in Fig. 8,  $\nu = 716Hz$  in Fig. 9, and  $\nu = 1000Hz$  in Fig. 10 respectively. (Rotational frequencies  $642Hz$  and  $716Hz$  are the spinning rates of the two fastest pulsars PSR1937+214 [3] and J1748-2446ad [5].) This formula for the Schwarzschild metric coincides with the one obtained in Newtonian gravity for a point mass  $M$  [2]. Eq. (22) implies

$$R_{max} = \chi \left( \frac{M}{1.4M_{\odot}} \right)^{1/3} km, \quad (23)$$

with  $\chi = 22.52$  for rotational frequency  $\nu = 642Hz$  (Fig. 8),  $\chi = 20.94$  for  $\nu = 716Hz$  (Fig. 9), and  $\chi = 16.76$  for  $\nu = 1000Hz$  (Fig. 10).

In Figs. 8-10 we observe that the range of the allowed masses supported by a given EOS for rapidly rotating neutron stars becomes narrower than the one of static configurations.

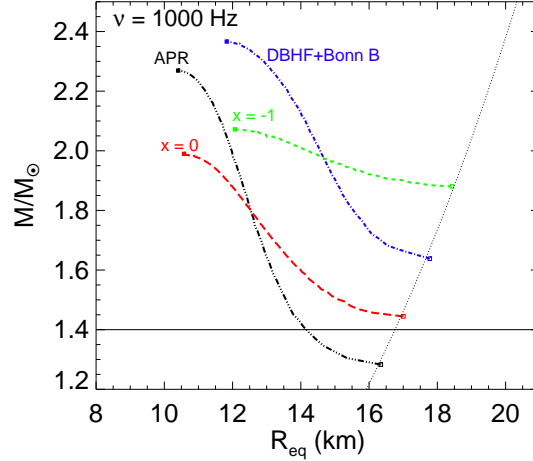


Figure 10: (Color online) Gravitational mass versus circumferential radius for neutron star models rotating at  $\nu = 1000Hz$ .

This effect becomes stronger with increasing frequency and depends upon the EOS. For instance, for models rotating at  $1000Hz$  (Fig. 10) for the  $x = -1$  EOS the allowed mass range is  $\sim 0.2M_{\odot}$ . As already discussed in the literature [2], this observation could explain why such rapidly rotating neutron stars are so rare – their allowed masses fall within a very narrow range.

## 5 Neutron star moment of inertia

In this section we turn our attention to the moment of inertia of neutron stars. Such studies are important and timely as they are related to astrophysical observations in the near future. In particular, the moment of inertia of pulsar A in the extremely relativistic neutron star binary PSR J0737-3039 [97] may be determined in a few years through detailed measurements of the periastron advance [98].

Employing the EOSs described briefly in section 2, we compute the neutron star moment of inertia with the *RNS* code. It solves the hydrostatic and Einstein’s field equations for mass distributions rotating rigidly under the assumption of stationary and axial symmetry about the rotational axis, and reflectional symmetry about the equatorial plane. *RNS* calculates the angular momentum  $J$  as [51]

$$J = \int T^{\mu\nu} \xi_{(\phi)}^{\nu} dV, \quad (24)$$

where  $T^{\mu\nu}$  is the energy-momentum tensor of stellar matter

$$T^{\mu\nu} = (\epsilon + P)u^{\mu}u^{\nu} + Pg^{\mu\nu}, \quad (25)$$

$\xi_{(\phi)}^{\nu}$  is the Killing vector in azimuthal direction reflecting axial symmetry, and  $dV = \sqrt{-g}d^3x$  is a proper 3-volume element ( $g \equiv \det(g_{\alpha\beta})$  is the determinant of the 3-metric). In Eq. (25)  $P$  is the pressure,  $\epsilon$  is the mass-energy density, and  $u^{\mu}$  is the unit time-like

four-velocity satisfying  $u^\mu u_\mu = -1$ . For axial-symmetric stars it takes the form  $u^\mu = u^t(1, 0, 0, \Omega)$ , where  $\Omega$  is the star's angular velocity. Under this condition Eq. (24) reduces to

$$J = \int (\epsilon + P) u^t (g_{\phi\phi} u^\phi + g_{\phi t} u^t) \sqrt{-g} d^3x \quad (26)$$

It should be noted that the moment of inertia cannot be calculated directly as an integral quantity over the source of gravitational field [51]. In addition, there exists no unique generalization of the Newtonian definition of the moment of inertia in General Relativity and therefore  $I = J/\Omega$  is a natural choice for calculating this important quantity.

For rotational frequencies much lower than the Kepler frequency (the highest possible rotational rate supported by a given EOS), i.e.  $\nu/\nu_k \ll 1$  ( $\nu = \Omega/(2\pi)$ ), the deviations from spherical symmetry are very small, so that the moment of inertia can be approximated from spherical stellar models. In what follows we review briefly this slow-rotation approximation, see e.g. Ref. [39]. In the slow-rotational limit the metric can be written in spherical coordinates as (in geometrized units  $G = c = 1$ )

$$ds^2 = -e^{2\phi(r)} dt^2 + \left(1 - \frac{2m(r)}{r}\right)^{-1} dr^2 - 2\omega r^2 \sin^2 \theta dt d\phi + r^2(d\theta^2 + \sin^2 \theta d\phi^2) \quad (27)$$

In the above equation  $m(r)$  is the total gravitational mass within radius  $r$  satisfying the usual equation

$$\frac{dm(r)}{dr} = 4\pi\epsilon(r)r^2 \quad (28)$$

and  $\omega(r) \equiv (d\phi/dt)_{ZAMO}$  is the Lense-Thirring angular velocity of a zero-angular-momentum observer (ZAMO). Up to first order in  $\omega$  all metric functions remain spherically symmetric and depend only on  $r$  [99]. In the stellar interior the Einstein's field equations reduce to

$$\frac{d\phi(r)}{dr} = m(r) \left[1 + \frac{4\pi r^3 P(r)}{m(r)}\right] \left[1 - \frac{2m(r)}{r}\right]^{-1} \quad (r < R_{star}) \quad (29)$$

and

$$\frac{1}{r^3} \frac{d}{dr} \left( r^4 j(r) \frac{d\bar{\omega}(r)}{dr} \right) + 4 \frac{dj(r)}{dr} \bar{\omega}(r) = 0 \quad (r < R_{star}), \quad (30)$$

with  $\bar{\omega} \equiv \Omega - \omega$  the dragging angular velocity (the angular velocity of the star relative to a local inertial frame rotating at  $\omega$ ) and

$$j \equiv \left(1 - \frac{2m(r)}{r}\right)^{1/2} e^{-\phi(r)} \quad (31)$$

Outside the star the metric functions become

$$e^{2\phi} = \left(1 - \frac{2M}{r}\right) \quad (r > R_{star}) \quad (32)$$

and

$$\omega = \frac{2J}{r^3} \quad (r > R_{star}), \quad (33)$$

where  $M = m(r = R) = 4\pi \int_0^R \epsilon(r') r'^2 dr'$  is the total gravitational mass and  $R$  is the stellar radius defined as the radius at which the pressure drops to zero ( $P(r = R) = 0$ ). At

the star's surface the interior and exterior solutions are matched by satisfying the appropriate boundary conditions

$$\bar{\omega}(R) = \Omega - \frac{R}{3} \left( \frac{d\bar{\omega}}{dr} \right)_{r=R} \quad (34)$$

and

$$\phi(r) = \frac{1}{2} \ln \left( 1 - \frac{2M}{R} \right) \quad (35)$$

The moment of inertia  $I = J/\Omega$  then can be computed from Eq. (26). With  $\Omega = u^\phi/u^t$  and retaining only first order terms in  $\omega$  and  $\Omega$ , the moment of inertia reads [99, 35]

$$I \approx \frac{8\pi}{3} \int_0^R (\epsilon + P) e^{-\phi(r)} \left[ 1 - \frac{2m(r)}{r} \right]^{-1} \frac{\bar{\omega}}{\Omega} r^4 dr \quad (36)$$

This slow-rotation approximation for the neutron-star moment of inertia neglects deviations from spherical symmetry and is independent of the angular velocity  $\Omega$  [99]. For neutron stars with masses greater than  $1M_\odot$  Lattimer and Schutz [100] found that, for slow-rotations, the moments of inertia computed through the above formalism (Eq. (36)) can be approximated very well by the following empirical relation:

$$I \approx (0.237 \pm 0.008) MR^2 \left[ 1 + 4.2 \frac{Mkm}{M_\odot R} + 90 \left( \frac{Mkm}{M_\odot R} \right)^4 \right] \quad (37)$$

The above equation is shown [100] to hold for a wide class of EOSs except for ones with appreciable degree of softening, usually indicated by achieving a maximum mass of  $\sim 1.6M_\odot$  or less. Since none of the EOSs employed in this paper exhibit such pronounced softening, Eq. (37) is a good approximation for the momenta of inertia of *slowly* rotating stars.

## 5.1 Slow rotation

If the rotational frequency is much smaller than the Kepler frequency, the deviations from spherical symmetry are negligible and the moment of inertia can be calculated applying the slow-rotation approximation discussed briefly above. For this case Lattimer and Schutz [100] showed that the moment of inertia can be very well approximated by Eq. (37). In Fig. 11 we display the moment of inertia as a function of stellar mass for slowly rotating neutron stars as computed with the empirical relation Eq. (37). As shown in Fig. 5, above  $\sim 1.0M_\odot$  the neutron star radius remains approximately constant before reaching the maximum mass supported by a given EOS. The moment of inertia ( $I \sim MR^2$ ) thus increases almost linearly with stellar mass for all models. Right before the maximum mass is achieved, the neutron star radius starts to decrease (Fig. 5), which causes the sharp drop in the moment of inertia observed in Fig. 11. Since  $I$  is proportional to the mass and the square of the radius, it is more sensitive to the density dependence of the nuclear symmetry energy, which determines the neutron star radius. Here we recall that the  $x = -1$  EOS has much stiffer symmetry energy (with respect to the one of the  $x = 0$  EOS), which results in neutron star models with larger radii and, in turn, momenta of inertia. For instance, for a ‘‘canonical’’ neutron star ( $M = 1.4M_\odot$ ), the difference in the moment of inertia is more

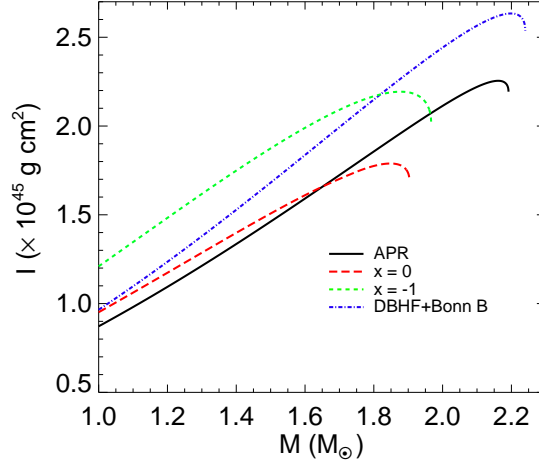


Figure 11: (Color online) Total moment of inertia of neutron stars estimated with Eq. (37). Taken from Ref. [60].

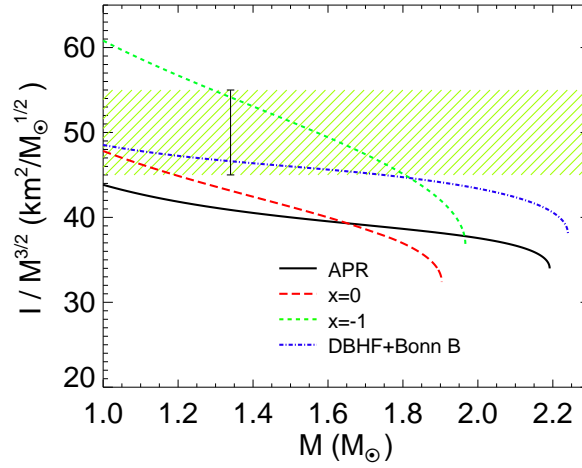


Figure 12: (Color online) The moment of inertia scaled by  $M^{3/2}$  as a function of the stellar mass  $M$ . The shaded band illustrates a 10% error of hypothetical  $I/M^{3/2}$  measurement of  $50 \text{ km}^2 M_\odot^{-1/2}$ . The error bar shows the specific case in which the mass is  $1.34 M_\odot$  (after Lattimer and Schutz [100]). Taken from Ref. [60].

than 30% with the  $x = 0$  and the  $x = -1$  EOSs. In Fig. 12 we take another view of the moment of inertia where  $I$  is scaled by  $M^{3/2}$  as a function of the stellar mass (after [100]).

The discovery of the extremely relativistic binary pulsar PSR J0737-3039A,B provides an unprecedented opportunity to test General Relativity and physics of pulsars [97]. Lattimer and Schutz [100] estimated that the moment of inertia of the A component of the system should be measurable with an accuracy of about 10%. Given that the masses of both stars are already accurately determined by observations, a measurement of the mo-

Table 5: Numerical results for PSR J0737-3039A ( $M_A = 1.338M_\odot$ ,  $\nu_A = 44.05Hz$ ).

EOS	$\epsilon_c(\times 10^{14}g\text{ cm}^{-3})$	$R_{eq}(km)$	$I(\times 10^{45}g\text{ cm}^2)$	$I^{LS}(\times 10^{45}g\text{ cm}^2)$
MDI(x=-1)	7.04	13.75 (13.64)	1.63	1.67
DBHF+Bonn B	7.34	12.56 (12.47)	1.57	1.43
MDI(x=0)	9.85	12.00 (11.90)	1.30	1.34
APR	9.58	11.60 (11.52)	1.25	1.26

The first column identifies the equation of state. The remaining columns exhibit the following quantities: central mass-energy density, equatorial radius (the numbers in the parenthesis are the radii of the spherical models; the deviations from sphericity due to rotation are  $\sim 1\%$ ), total moment of inertia, total moment of inertia  $I^{LS}$  as computed with Eq. (37).

ment of inertia of even one neutron star could have enormous importance for the neutron star physics [100]. (The significance of such a measurement is illustrated in Fig. 12. As pointed by [100], it is clear that very few EOSs would survive these constraints.) Thus, theoretical predictions of the moment of inertia are very timely. Calculations of the moment of inertia of pulsar A ( $M_A = 1.338M_\odot$ ,  $\nu_A = 44.05Hz$ ) have been reported by Morrison et al. [99] and Bejger et al. [98]. In Table 5 we show the moment of inertia (and other selected quantities) of PSR J0737-3039A computed with the *RNS* code using the EOSs employed in this study. Our results with the APR EOS are in very good agreement with those by [99] ( $I^{APR} = 1.24 \times 10^{45}g\text{ cm}^2$ ) and [98] ( $I^{APR} = 1.23 \times 10^{45}g\text{ cm}^2$ ). In the last column of Table 5 we also include results computed with the empirical relation (Eq. (37)). From a comparison with the results from the exact numerical calculation we conclude that Eq. (37) is an excellent approximation for the moment of inertia of slowly-rotating neutron stars. (The average uncertainty of Eq. (37) is  $\sim 2\%$ , except for the DBHF+BonnB EOS for which it is  $\sim 8\%$ .) Our results (with the MDI EOS) allowed us to constrain the moment of inertia of pulsar A to be in the range  $I = (1.30 - 1.63) \times 10^{45}(g\text{ cm}^2)$ .

## 5.2 Rapid rotation

In this subsection we turn our attention to the moment of inertia of rapidly rotating neutron stars. In Fig. 13 we show the moment of inertia as a function of stellar mass for neutron star models spinning at the mass-shedding (Kepler) frequency. The numerical calculation is performed with the *RNS* code. We observe that the moments of inertia of rapidly rotating neutron stars are significantly larger than those of slowly rotating models (for a fixed mass). This is easily understood in terms of the increased (equatorial) radius (Fig. 5).

We also compute the moments of inertia of pulsars spinning at 642Hz, 715Hz, and 1000Hz (642Hz [3] and 716Hz [6] are the rotational frequencies of the fastest pulsars as of today). The numerical results are presented in Fig. 14. As demonstrated by Bejger et al. [2] and most recently by Krastev et al. [59], the range of the allowed masses supported by a given EOS for rapidly rotating neutron stars becomes narrower than the one for static configurations. The effect becomes stronger with increasing frequency and depends upon the EOS. This is also illustrated in Fig. 14, particularly in panel (c). Additionally, the



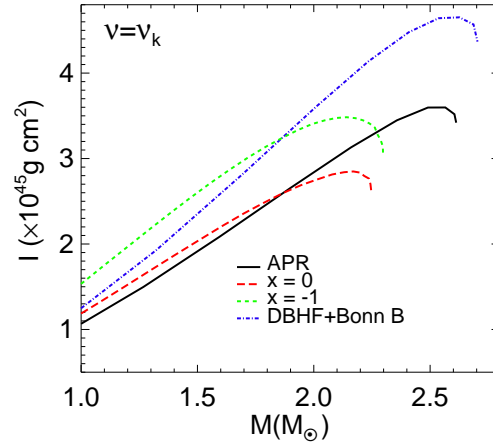


Figure 13: (Color online) Total moment of inertia for Keplerian models. The neutron star sequences are computed with the *RNS* code. Taken from Ref. [60].

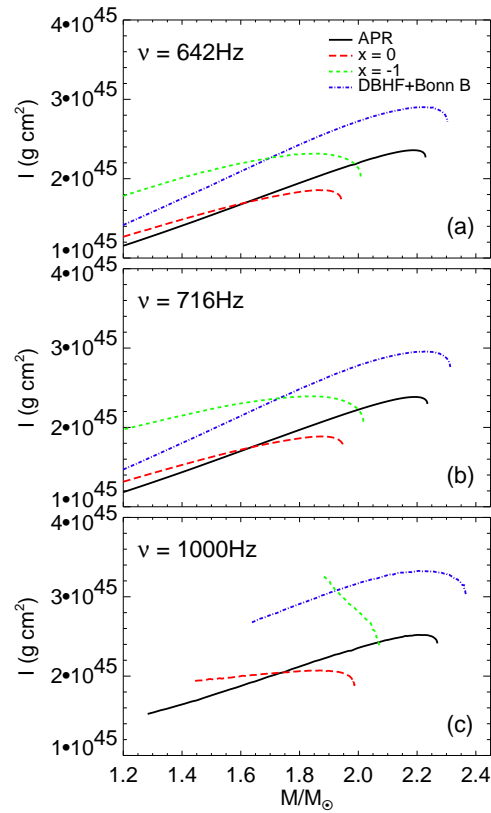


Figure 14: (Color online) Total moment of inertia as a function of stellar mass for models rotating at 642Hz (a), 716Hz (b), and 1000Hz (c). Data is partially taken from Ref. [60].

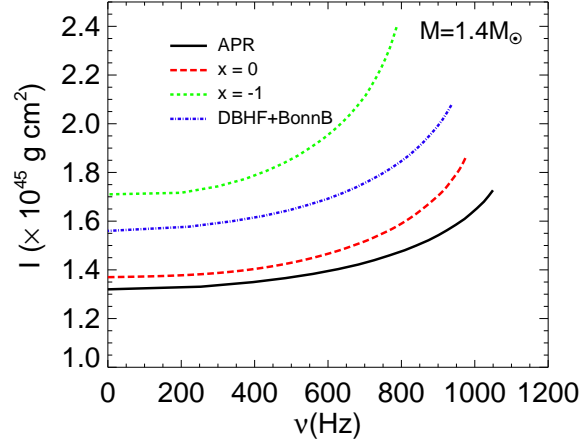


Figure 15: (Color online) Total moment of inertia as a function of rotational frequency for stellar models with mass  $M = 1.4M_{\odot}$ . Taken from Ref. [60].

moment of inertia shows increase with rotational frequency at a rate dependent upon the details of the EOS. This is best seen in Fig. 15 where we display the moment of inertia as a function of the rotational frequency for stellar models with a fixed mass ( $M = 1.4M_{\odot}$ ).

The neutron star sequences shown in Fig. 14 are terminated at the mass-shedding frequency. At the lowest frequencies the moment of inertia remains roughly constant for all EOSs (which justifies the application of the slow-rotation approximation and Eq. (37)). As the stellar models approach the Kepler frequency, the moment of inertia exhibits a sharp rise. This is attributed to the large increase of the circumferential radius as the star approaches the “mass-shedding point”. As pointed by Friedman et al. [92], properties of rapidly rotating neutron stars display greater deviations from those of spherically symmetric (static) stars for models computed with stiffer EOSs. This is because such models are less centrally condensed and gravitationally bound. This also explains why the momenta of inertia of rapidly rotating neutron star configurations from the  $x = -1$  EOS show the greatest deviation from those of static models.

### 5.3 Fractional moment of inertia of the neutron star crust

As it was discussed extensively by Lattimer and Prakash [35] (and others), the neutron star crust thickness might be measurable from observations of pulsar glitches, the occasional disrupts of the otherwise extremely regular pulsation from magnetized, rotating neutron stars. The canonical model of Link et al. [101] suggests that glitches are due to the angular momentum transfer from superfluid neutrons to normal matter in the neutron star crust, the region of the star containing nuclei and nucleons that have dripped out of nuclei. This region is bound by the neutron drip density at which nuclei merge into uniform nucleonic matter. Link et al. [101] concluded from the observations of the Vela pulsar that at least 1.4% of the total moment of inertia resides in the crust of the Vela pulsar. For slowly rotating neutron stars, applying several realistic hadronic EOSs that permit maximum masses of at least  $\sim 1.6M_{\odot}$  Lattimer and Prakash [35] found that the fractional moment of inertia,  $\Delta I/I$ ,

Table 6: Transition densities and pressures for the EOSs used in this paper.

EOS	MDI(x=0)	MDI(x=-1)	APR	DBHF+Bonn B
$\rho_t(\text{fm}^{-3})$	0.091 (0.095)	0.093 (0.092)	0.087	0.100
$P_t(\text{MeV fm}^{-3})$	0.645	0.982	0.513	0.393

The first row identifies the equation of state. The remaining rows exhibit the following quantities: transition density, transition pressure. The numbers in the parenthesis are the transition densities calculated by Kubis [102].

can be expressed approximately as

$$\frac{\Delta I}{I} \simeq \frac{28\pi P_t R^3}{3Mc^2} \frac{(1 - 1.67\beta - 0.6\beta^2)}{\beta} \left[ 1 + \frac{2P_t(1 + 5\beta - 14\beta^2)}{\rho_t m_b c^2 \beta^2} \right]^{-1} \quad (38)$$

In the above equation  $\Delta I$  is the moment of inertia of the neutron star crust,  $I$  is the total moment of inertia,  $\beta = GM/Rc^2$  is the compactness parameter,  $m_b$  is the average nucleon mass,  $\rho_t$  is the transition density at the crust-core boundary, and  $P_t$  is the transition pressure.

The determination of the transition density itself is a very complicated problem. Different approaches often give quite different results. Similar to determining the critical density for the spinodal decomposition for the liquid-gas phase transition in nuclear matter, for uniform *npe*-matter, Lattimer and Prakash [35] and more recently Kubis [102] have evaluated the crust transition density by investigating when the incompressibility of *npe*-matter becomes negative, i.e

$$K_\mu = \rho^2 \frac{d^2 E_0}{d\rho^2} + 2\rho \frac{dE_0}{d\rho} + \delta^2 \left[ \rho^2 \frac{d^2 E_{sym}}{d\rho^2} + 2\rho \frac{dE_{sym}}{d\rho} - 2E_{sym}^{-1} \left( \rho \frac{dE_{sym}}{d\rho} \right)^2 \right] < 0 \quad (39)$$

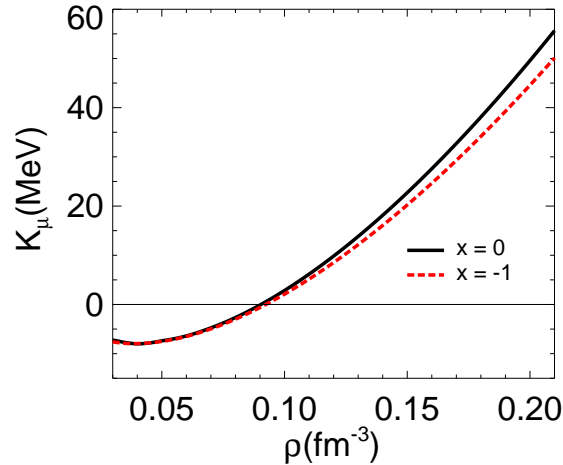


Figure 16: (Color online) The incompressibility,  $K_\mu$ , as a function of baryon density  $\rho$ . Taken from Ref. [60].

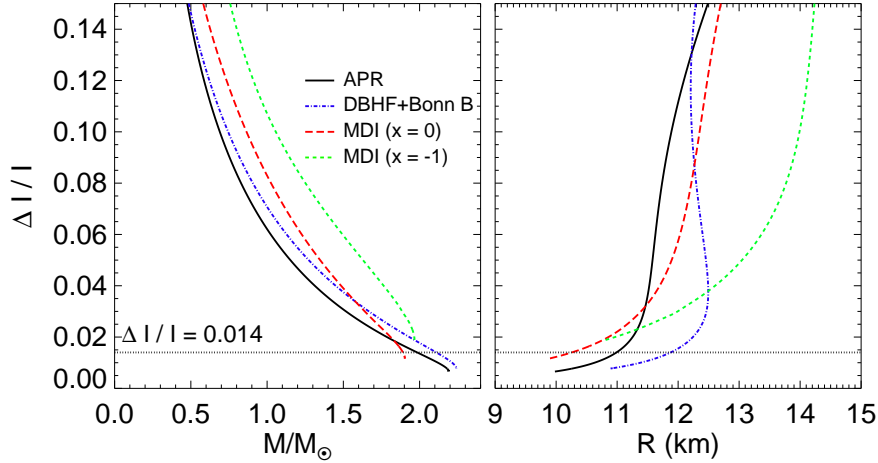


Figure 17: (Color online) The fractional moment of inertia of the neutron star crust as a function of the neutron star mass (left panel) and radius (right panel) estimated with Eq. (39). The constraint from the glitches of the Vela pulsar is also shown. Taken from Ref. [60].

(see Fig. 16) where  $E_0(\rho)$  is the EOS of symmetric nuclear matter,  $E_{sym}$  is the nuclear symmetry energy, and  $\delta = (\rho_n - \rho_p)/(\rho_n + \rho_p)$  is the asymmetry parameter. Using this approach and the MDI interaction, Kubis [102] found the transition density of 0.119, 0.092, 0.095 and  $0.160 fm^{-3}$  for the  $x$  parameter of 1, 0,  $-1$  and  $-2$ , respectively. Similarly, we have calculated the transition densities and pressures for the EOSs employed in this work. Our results are summarized in Table 6. We find good agreement between our results and those by Kubis [102] with the MDI interaction. It is interesting to notice that the transition densities predicted by all EOSs are in the same density range explored by heavy-ion reactions at intermediate energies. The MDI interaction with  $x = 0$  and  $x = -1$  constrained by the available data on isospin diffusion in heavy-ion reaction at intermediate energies thus limits the transition density rather tightly in the range of  $\rho_t = [0.091 - 0.093](fm^{-3})$ . It is worth noticing, however, that the transition density is estimated here by using the parabolic approximation of the EOS for isospin asymmetric nuclear matter. Relaxing this approximation, using both dynamical and thermodynamical approaches, the transition density and pressure have been studied in great detail in Ref. [56]. A somewhat lower values of  $\rho_t = [0.040 - 0.065](fm^{-3})$  were obtained. Nevertheless, to be consistent with the rest of the study in this review, we stick to the parabolic approximation of the EOS in studying the  $\Delta I/I$ .

The fractional momenta of inertia  $\Delta I/I$  of the neutron star crusts are shown in Fig. 17 as computed through Eq. (38) with the parameters listed in Table 6. It is seen that the condition  $\Delta I/I > 0.014$  extracted from studying the glitches of the Vela pulsar does put a strict lower limit on the radius for a given EOS. It also limits the maximum mass to be less than about  $2M_\odot$  for all of the EOSs considered. Similar to the total momenta of inertia the ratio  $\Delta I/I$  changes more sensitively with the radius as the EOS is varied.

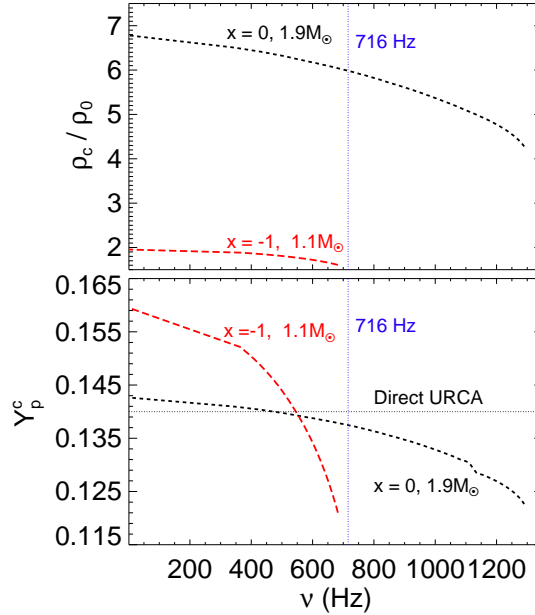


Figure 18: (Color online) Density (upper panel) and proton fraction (lower panel) versus rotational frequency for fixed neutron star mass. Taken from Ref. [59].

## 6 Rotation and proton fraction

Finally, we study the effect of (fast) rotation on the proton fraction in the neutron star core. In Fig. 18 we show the central baryon density (upper frame) and central proton fraction (lower frame) as a function of the rotational frequency for fixed-mass models. Predictions from both  $x = 0$  and  $x = -1$  EOSs are shown. We observe that central density decreases with increasing frequency. This reduction is more pronounced in heavier neutron stars. Most importantly, we also observe decrease in the proton fraction  $Y_p^c$  in the star's core. We recall that large proton fraction (above  $\sim 0.14$  for  $npe\mu$ -stars) leads to fast cooling of neutron stars through direct Urca reactions. Our results demonstrate that depending on the stellar mass and rotational frequency, the central proton fraction could, in principle, drop below the threshold for the direct *nucleonic* Urca channel and thus making the fast cooling in rotating neutron stars impossible. The masses of the models shown in Fig. 18 are chosen so that the proton fraction in stellar core is just above the direct Urca limit for the *static* configurations, see Fig. 19 upper and lower frames. The stellar sequences in Fig. 18 are terminated at the Kepler (mass-shedding) frequency. In both cases the central proton fraction drops below the direct Urca limit at frequencies lower than that of PSR J1748-244ad [5]. This implies that the fast cooling can be effectively blocked in millisecond pulsars depending on the exact mass and spin rate. It might also explain why heavy neutron stars (could) exhibit slow instead of fast cooling. For instance, with the  $x = 0$  EOS (with softer symmetry energy) for a neutron star of mass approximately  $1.9M_\odot$ , the Direct Urca channel closes at  $\nu \approx 470\text{Hz}$ . On the other hand, with the  $x=-1$  EOS (with stiffer symmetry energy) the direct Urca channel can close only for low mass neutron stars, in fact only for

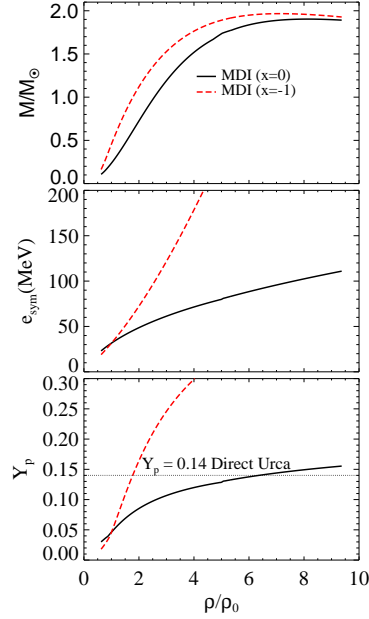


Figure 19: (Color online) Neutron star mass (upper panel), nuclear symmetry energy (middle panel) and proton fraction (lower panel) versus baryon density. Predictions from the MDI ( $x=-1,0$ ) are shown. Taken from Ref. [59].

masses well below the canonical mass of  $1.4M_{\odot}$ . This is due to the much stiffer symmetry energy (see Fig. 19 middle frame) because of which the direct Urca threshold (Fig. 19 lower frame) is reached at much lower densities and stellar masses (Fig. 19 upper frame).

Before closing the discussion in this section a few comments are in order. In the present study we do not consider "exotic" states of matter in neutron stars. On the other hand, due to the rapid rise of the baryon chemical potentials several other species of particles, such as strange hyperons  $\Lambda^0$  and  $\Sigma^-$ , are expected to appear once their mass thresholds are reached [103]. The appearance of hyperonic degrees of freedom lowers the energy-per-particle in the stellar medium and causes more centrally condensed configurations with lower masses and radii. Additionally, hyperons help the condition for *nucleonic* direct Urca process to be satisfied at lower densities due to the increased proton fraction [104], and depending on their exact concentrations could potentially contribute to the fast cooling of the star through *hyperonic* direct Urca processes [105]. These considerations would alter the balance between the curves in Fig. 19 and ultimately the results displaced in Fig. 18 in favor of the direct Urca process, i.e. smaller masses and higher frequencies would be necessary to close the fast cooling channel. This is due to the fact that the overall impact of (rapid) rotation on the neutron star structure is smaller for more centrally condensed models resulting from "softer" EOSs [92]. Therefore, for such models there is smaller deviation from properties and structure of static configurations. In addition, at even higher densities matter is expected to undergo a transition to quark-gluon plasma [4, 103], which favors a fast cooling through enhanced nucleonic direct Urca and quark direct Urca processes, see

e.g., Ref. [105].

## 7 Constraining gravitational waves from elliptically deformed pulsars

Gravitational waves are tiny disturbances in space-time and are a fundamental, although not yet directly confirmed, prediction of General Relativity. They can be triggered in cataclysmic events involving (compact) stars and/or black holes. They could even have been produced during the very early Universe, well before any stars had been formed, merely as a consequence of the dynamics and expansion of the Universe. Because gravity interact extremely weakly with matter, gravitational waves would carry a genuine picture of their sources and thus provide undisturbed information that no other messenger can deliver [106]. Gravitational wave astrophysics would open an entirely new non-electromagnetic window making it possible to probe physics that is hidden or dark to current electromagnetic observations [107].

(Rapidly) rotating neutron stars could be one of the major candidates for sources of continuous gravitational waves in the frequency bandwidth of the LIGO [108] and VIRGO (e.g. Ref. [109]) laser interferometric detectors. It is well known that a rotating object self-bound by gravity and which is perfectly symmetric about the axis of rotation does not emit gravitational waves. In order to generate gravitational radiation over extended period of time, a rotating neutron star must have some kind of long-living axial asymmetry [110]. Several mechanisms leading to such an asymmetry have been studied in the literature: (1) Since the neutron star crust is solid, its shape might not be necessarily symmetric, as it would be for a fluid, with asymmetries supported by anisotropic stress built up during the crystallization period of the crust [111]. (2) Additionally, due to its violent formation (supernova) or due to its environment (accretion disc), the rotational axis may not coincide with a principal axis of the moment of inertia of the neutron star which make the star precess [112]. Even if the star remains perfectly symmetric about the rotational axis, since it precesses, it emits gravitational waves [112, 113]. (3) Also, the extreme magnetic fields presented in a neutron star cause magnetic pressure (Lorenz forces exerted on conducting matter) which can distort the star if the magnetic axis is not aligned with the axis of rotation [114], which is widely supposed to occur in order to explain the pulsar phenomenon. Several other mechanisms exist that can produce gravitational waves from neutron stars. For instance, accretion of matter on a neutron star can drive it into a non-axisymmetric configuration and power steady radiation with a considerable amplitude [115]. This mechanism applies to a certain class of neutron stars, including accreting stars in binary systems that have been spun up to the first instability point of the so-called Chandrasekhar-Friedman-Schutz (CFS) instability [116]. Also, Andersson [117] suggested a similar instability in  $r$ -modes of (rapidly) rotating relativistic stars. It has been shown that the effectiveness of these instabilities depends on the viscosity of stellar matter which in turn is determined by the star's temperature.

Gravitational waves are characterized by tiny dimensionless strain amplitude, which depends on the degree to which the neutron star is deformed from axial symmetry which, in turn, depends upon the equation of state (EOS) of neutron-rich stellar matter. As already mentioned, presently the EOS of matter under extreme conditions (densities, pressures and

isospin asymmetries) is still rather uncertain, mainly due to the poorly known density dependence of the nuclear symmetry energy,  $E_{sym}(\rho)$ , e.g. [9]. Applying several nucleonic EOSs (discussed in section 2), we calculate the gravitational wave strain amplitude for selected neutron star configurations. Particular attention is paid to predictions with the EOS partially constrained by the nuclear laboratory data. These results set an upper limit on the strain amplitude of gravitational radiation expected from rotating neutron stars.

The pulsar population is such that most have spin frequencies that fall below the sensitivity band of current detectors. In the future, the low-frequency sensitivity of VIRGO [118] and Advanced LIGO [119] should allow studies of a significantly larger sample of pulsars. Moreover, LISA (the Laser Interferometric Space Antenna) is currently being jointly designed by NASA in the United States and ESA (the European Space Agency), and will be launched into orbit in the near future providing an unprecedented instrument for gravitational waves search and detection [107]. The discussion in this section is (mainly) based on Ref. [61].

### 7.1 Formalism relating the EOS of neutron-rich matter to the strength of gravitational waves from slowly rotating neutron stars

In the following we review briefly the formalism used to calculate the gravitational wave strain amplitude from slowly rotating neutron stars. A spinning neutron star is expected to emit GWs if it is not perfectly symmetric about its rotational axis. As already mentioned, non-axial asymmetries can be achieved through several mechanisms such as elastic deformations of the solid crust or core or distortion of the whole star by extremely strong misaligned magnetic fields. Such processes generally result in a triaxial neutron star configuration [108] which, in the quadrupole approximation and with rotation and angular momentum axes aligned, would cause gravitational waves at *twice* the star's rotational frequency [108]. These waves have characteristic strain amplitude at the Earth's vicinity (assuming an optimal orientation of the rotation axis with respect to the observer) of [120]

$$h_0 = \frac{16\pi^2 G}{c^4} \frac{\epsilon I_{zz} \nu^2}{r}, \quad (40)$$

where  $\nu$  is the neutron star rotational frequency,  $I_{zz}$  its principal moment of inertia,  $\epsilon = (I_{xx} - I_{yy})/I_{zz}$  its equatorial ellipticity, and  $r$  its distance to Earth. The ellipticity is related to the neutron star maximum quadrupole moment (with  $m = 2$ ) via [121]

$$\epsilon = \sqrt{\frac{8\pi}{15} \frac{\Phi_{22}}{I_{zz}}}, \quad (41)$$

where for *slowly* rotating (and static) neutron stars  $\Phi_{22}$  can be written as [121]

$$\Phi_{22,max} = 2.4 \times 10^{38} g \text{ cm}^2 \left( \frac{\sigma}{10^{-2}} \right) \left( \frac{R}{10 \text{ km}} \right)^{6.26} \left( \frac{1.4 M_\odot}{M} \right)^{1.2} \quad (42)$$

In the above expression  $\sigma$  is the breaking strain of the neutron star crust which is rather uncertain at present time. Earlier studies have estimated  $\sigma$  to be in the range  $\sigma = [10^{-5} - 10^{-2}]$  [120]. More recently, using molecular dynamics simulations, it was estimated to be about 0.1 which is considerably larger than the previous findings [122]. In our work [61], we



have used  $\sigma = 10^{-2}$ , which, compared to the latest estimate [122], is rather conservative. Nevertheless, our results are simply amplified by a factor of 100 if we apply the estimate by Horowitz et al. [122] in our calculations. From Eqs. (40) and (41) it is clear that  $h_0$  does not depend on the moment of inertia  $I_{zz}$ , and that the total dependence upon the EOS is carried by the quadrupole moment  $\Phi_{22}$ . Thus Eq. (40) can be rewritten as

$$h_0 = \chi \frac{\Phi_{22} \nu^2}{r}, \quad (43)$$

with  $\chi = \sqrt{2045\pi^5/15G/c^4}$ . Eq. (43) establishes the link between the gravitational wave strain amplitude and the EOS of neutron-rich matter—the EOS is the main ingredient for determining the neutron star properties, including its quadrupole moment. In a recent work [60] we have calculated the neutron star moment of inertia of both static and (rapidly) rotating neutron stars. For slowly rotating neutron stars Lattimer and Schutz [100] derived an empirical relation (Eq. (37)) for  $I_{zz}$  which is shown to hold for a wide class of equations of state which do not exhibit considerable softening and for neutron star models with masses above  $1M_\odot$  [100]. Using Eq. (37) to calculate the neutron star moment of inertia and Eq. (42) the corresponding quadrupole moment, the ellipticity  $\epsilon$  can be readily computed (via Eq. (41)). Since the global properties of spinning neutron stars (in particular the moment of inertia) remain approximately constant for rotating configurations at frequencies up to  $\sim 300Hz$  [60], the above formalism can be readily employed to estimate the gravitational wave strain amplitude, provided one knows the exact rotational frequency and distance to Earth, and that the frequency is relatively low (below  $\sim 300Hz$ ). These estimates are then to be compared with the current upper limits for the sensitivity of the laser interferometric observatories (e.g. LIGO).

## 7.2 Gravitational waves from *slowly* rotating neutron stars

We calculate the gravitational wave strain amplitude  $h_0$  for several selected pulsars with rotational frequencies  $\sim 200Hz$  and relatively close to Earth, employing several nucleonic equations of state. We assume a simple model of stellar matter of nucleons and light leptons (electrons and muons) in beta-equilibrium. The equations of state that we employ here have been discussed in section 2 and shown in Fig. 3.

Fig. 20 displays the neutron star quadrupole moment (left panel) and ellipticity (right panel). The quadrupole moment is calculated through Eq. (42) and the ellipticity through Eq. (41). Note that Eq. (42) is valid only for *slowly* rotating neutron star models. We notice that  $\Phi_{22}$  decreases with increasing stellar mass for all EOSs considered in this study. The rate of this decrease depends upon the EOS and is largest for the  $x = -1$  EOS. This behavior is easily understood in terms of the increased central density with stellar mass – more massive stars are more compact and, since the quadrupole moment is a measure of the star’s deformation (see Eq. (41)), they are also less deformed with respect to less centrally condensed models. Moreover, it is well known that the mass is mainly determined by the symmetric part of the EOS while the radius of a neutron star is strongly affected by the density slope of the symmetry energy. More quantitatively, an EOS with a stiffer symmetry energy, such as the  $x = -1$  EOS, results in less compact stellar models, and hence more deformed pulsars. Here we recall specifically that the  $x = -1$  EOS yields

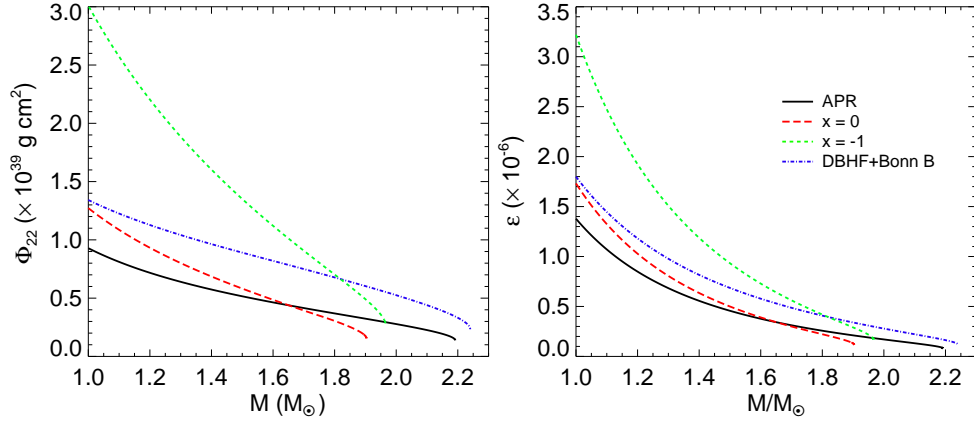


Figure 20: (Color online) Neutron star quadrupole moment (left panel) and ellipticity (right panel). Taken from Ref. [61].

neutron star configurations with larger radii than those of models form the rest of the EOSs considered in this study (e.g. see Fig. 5). These results are consistent with previous findings which suggest that more compact neutron star models are less altered by rotation, e.g. see Ref. [92]. Consequently, it is reasonable also to expect such configurations to be more “resistant” to any kind of deformation. The neutron star ellipticity,  $\epsilon$ , is shown as a function of the neutron star mass (Fig. 20, right panel). Since  $\epsilon$  is proportional to the quadrupole moment  $\Phi_{22}$  (scaled by the moment of inertia  $I_{zz}$ ), it decreases with increasing stellar mass. The results shown in the right panel of Fig. 20 are consistent with the maximum ellipticity  $\epsilon_{max} \approx 2.4 \times 10^{-6}$  corresponding to the largest crust “mountain” one could expect on a neutron star [120, 123]. (The estimate of  $\epsilon_{max}$  in Refs. [120, 123] has been obtained assuming breaking strain of the crust  $\sigma = 10^{-2}$ , as we have assumed in the present paper in calculating the neutron star quadrupole moment.)

In Fig. 21 we display the GW strain amplitude,  $h_0$ , as a function of stellar mass. Predictions are shown for three selected millisecond pulsars, which are relatively close to Earth ( $r < 0.4 \text{ kpc}$ ), and have rotational frequencies below  $300 \text{ Hz}$  so that the corresponding momenta of inertia and quadrupole moments can be computed approximately via Eqs. (37) and (42) respectively. The properties of these pulsars (of interest to this study) are summarized in Table 7. The error bars in Fig. 21 between the  $x = 0$  and  $x = -1$  EOSs provide a constraint on the *maximal* strain amplitude of the gravitational waves emitted by the millisecond pulsars considered here. The specific case shown in the figure is for neutron star models of  $1.4 M_\odot$ . Depending on the exact rotational frequency, distance to detector, and details of the EOS, the *maximal*  $h_0$  is in the range  $\sim [0.4 - 1.5] \times 10^{-24}$ . These estimates do not take into account the uncertainties in the distance measurements. They also should be regarded as upper limits since the quadrupole moment (Eq. (42)) has been calculated with  $\sigma = 10^{-2}$  (where  $\sigma$  can go as low as  $10^{-5}$ ). Here we recall that the mass of PSR J0437-4715 (Fig. 21 right panel) is  $1.3 \pm 0.2 M_\odot$  [125]. (Another mass constraint,  $1.58 \pm 0.18 M_\odot$ , was given previously by van Straten et al. [126].) The results shown in Fig. 21 suggest that the GW strain amplitude depends on the EOS of stellar matter, where this dependence is stronger for lighter neutron star models. In addition, it is also greater for stellar configura-

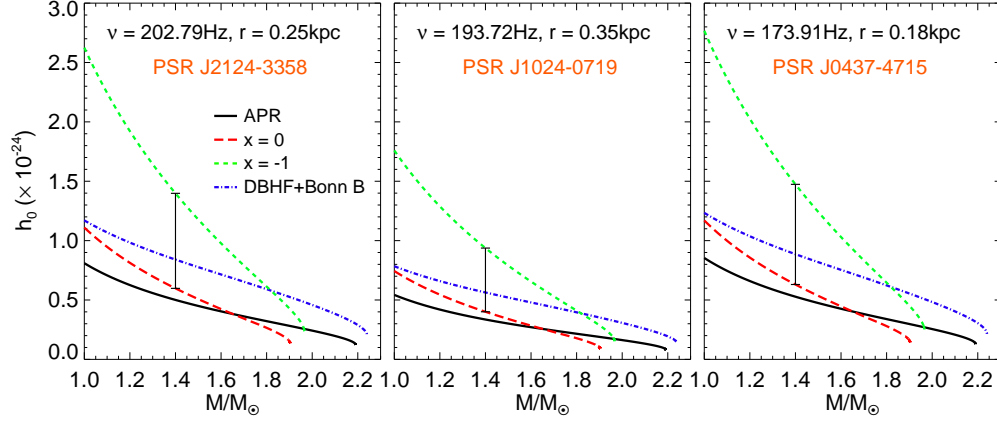


Figure 21: (Color online) Gravitational-wave strain amplitude as a function of the neutron star mass. The error bars between the  $x = 0$  and  $x = -1$  EOSs provide a limit on the strain amplitude of the gravitational waves to be expected from these neutron stars, and show a specific case for stellar models of  $1.4M_{\odot}$ . Taken from Ref. [61].

Table 7: Properties of the pulsars considered in this study.

Pulsar	$\nu(Hz)$	$M(M_{\odot})$	$r(kpc)$	Reference
PSR J2124-3358	202.79	-	0.25	[124]
PSR J1024-0719	193.72	-	0.35	[124]
PSR J0437-4715	173.91	$1.3 \pm 0.2$	0.18	[125, 126]

The first column identifies the pulsar. The remaining columns exhibit the following quantities: rotational frequency; mass (if known); distance to Earth; corresponding references. Notice that only the mass of PSR J0437-4715 is known from orbital dynamics [126, 125] (as the pulsar has a low-mass white dwarf companion). The masses of PSRs J2124-3358 and J1024-0719 are presently unknown as they are both isolated neutron stars [124].

tions computed with stiffer EOS. As explained, such models are less compact and thus less gravitationally bound. As a result, they could be more easily deformed by rotation or/and other deformation driving mechanisms and phenomena, and therefore are expected to emit stronger gravitational radiation (Eq. (40)).

In Fig. 22 we take another view of the results shown in Fig. 21. We display the maximal GW strain amplitude as a function of the GW frequency and compare our predictions with the best current detection limit of LIGO. The specific case shown is for neutron star models with mass  $1.4M_{\odot}$  computed with the  $x = 0$  and  $x = -1$  EOSs. Since these EOSs are constrained by the available nuclear laboratory data they provide a limit on the possible neutron star configurations and thus gravitational emission from them. The results shown in Fig. 22 would suggest that presently the gravitational radiation from the three selected pulsars should be within the detection capabilities of LIGO. The fact that such a detection

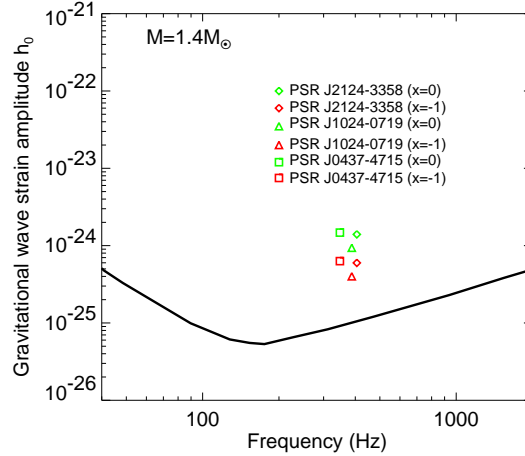


Figure 22: (Color online) Gravitational wave strain amplitude as a function of the gravitational wave frequency. The characters denote the strain amplitude of the GWs expected to be emitted from spinning neutron stars ( $\nu < 300 \text{ Hz}$ ) with mass  $1.4M_{\odot}$ . Solid line denotes the current upper limit of the LIGO sensitivity. Adapted from Ref. [108].

has not been made yet deserves a few comments at this point. First, as we mentioned, in the present calculation we assume breaking strain of the neutron star crust  $\sigma = 10^{-2}$  which might be too optimistic. As pointed by Haskell et al. [120], we are still away from testing more conservative models and if the true value of  $\sigma$  lies in the low end of its range, we would be still far away from a direct detection of a gravitational wave signal. Second, while we have assumed a specific neutron star mass of  $1.4M_{\odot}$ , Fig. 21 tells us that  $h_0$  decreases with increasing stellar mass, i.e. heavier neutron stars will emit weaker GWs. Here we recall that from the selected pulsars only the mass of PSR J0437-4715 is known (within some accuracy [125, 126]). The masses of PSR J2124-3358 and PSR J1024-0719 are unknown. Third, in the present study we assume a very simple model of stellar matter consisting only beta equilibrated nucleons and light leptons (electrons and muons). On the other hand, in the core of neutron stars conditions are such that other more exotic species of particles could readily abound. Such novel phases of matter would soften considerably the EOS of stellar medium [103] leading to ultimately more compact and gravitationally tightly bound objects which could withstand larger deformation forces (and torques). Lastly, the existence of quark stars, truly exotic self-bound compact objects, is not excluded from further considerations and studies. Such stars would be able to resist huge forces (such as those resulting from extremely rapid rotation beyond the Kepler, or mass-shedding, frequency) and as a result retain their axial symmetric shapes effectively dumping the gravitational radiation (e.g. Ref. [4]). At the end, we recall that Eq. (40) implies that the best possible candidates for gravitational radiation (from spinning relativistic stars) are *rapidly* rotating pulsars relatively close to Earth ( $h_0 \sim \Phi_{22}\nu^2/r$ ). Increasing rotational frequency (and/or decreasing distance to detector,  $r$ ) would alter the results shown in Figs. 21 and 22 in favor of a detectable signal by the current observational facilities (e.g. LIGO). On the other hand, for more realistic and quantitative calculations, the neutron star quadrupole moment must

Table 8: Properties of the *rapidly rotating* pulsars considered in this study. The first column identifies the pulsar. The remaining columns exhibit the following quantities: rotational frequency; first derivative of the rotational frequency; distance to Earth; corresponding reference.

Pulsar	$\nu(Hz)$	$\dot{\nu}(Hz\ s^{-1})$	$r(kpc)$	Reference
PSR B1937+21	641.93	$-4.33 \times 10^{-14}$	3.60	[3, 130]
PSR J1748-2446ad	716.35	–	8.70	[5, 131]

be calculated numerically exactly by solving the Einstein field equations for rapidly rotating neutron stars. (Such calculations have been reported, for instance, by Laarakkers and Piosson [127].)

### 7.3 Gravitational waves from *rapidly rotating* neutron stars

For rapidly rotating neutron stars the estimate of the quadrupole deformation in Eq. (42) is no longer valid. Moreover, the moment of inertia has to be calculated differently as well. Often, one uses the spin-down rate to estimate the strain amplitude for fast pulsars. Provided that the spin-down rate,  $\dot{\nu}$ , for a given pulsar is known,  $h_0$  could be estimated from [128]

$$h_0^{sd} = \frac{5}{2} \left( \frac{GI_{zz}|\dot{\nu}|}{c^3 r^2 \nu} \right)^{1/2}. \quad (44)$$

Here we should mention that in such calculations one assumes that the *only* mechanism contributing to the pulsar’s observed spin-down is gravitational radiation. However, other mechanisms could also account for the star’s observed decrease in rotational frequency such as magnetic dipole radiation, and particle acceleration in the magnetosphere [129]. Despite these uncertainties, calculations of gravitational wave strain amplitude through Eq. (44) are still important because, in addition to providing a rather conservative upper limit on the expected gravitational radiation, they also serve to estimate another very uncertain but important quantity – the ellipticity  $\epsilon$ . So far the fastest pulsars reported are the PSR B1937+21 [3] and PSR J1748-2446ad [5]. Their known properties are summarized in Table 8.

The *RNS* code [46] was used to calculate the principal moment of inertia (and other properties) of rapidly rotating neutron stars. The neutron star moment of inertia for the two fastest pulsars is shown in Fig 14. Panel (a) shows the moment of inertia of PSR B1937+21 and panel (b) displays the moment of inertia of PSR J1748-2446ad. As already observed previously, the moment of inertia increases with rotational frequency, while the range of possible neutron star configurations decreases (see, for instance, Refs. [59, 60]).

A particularly interesting example is the neutron star rotating at 642 Hz [3]. Since its first observation in 1982, this pulsar has been studied extensively and an observed spin-down rate has been measured (see Table 1). Using the spin-down rate, an upper limit on the gravitational wave strain amplitude was obtained. The spin-down rate corresponds to a loss in kinetic energy at a rate of  $\dot{E} = 4\pi^2 I_{zz} \nu |\dot{\nu}| \sim [0.6 - 3.1] \times 10^{36} \text{ erg/s}$ , depending on the EOS. Assuming that the energy loss is completely due to the gravitational radiation, the gravitational wave strain amplitude can be calculated through Eq. (44). Similar calculations for this pulsar and others with an observed spin-down rate have been performed in the

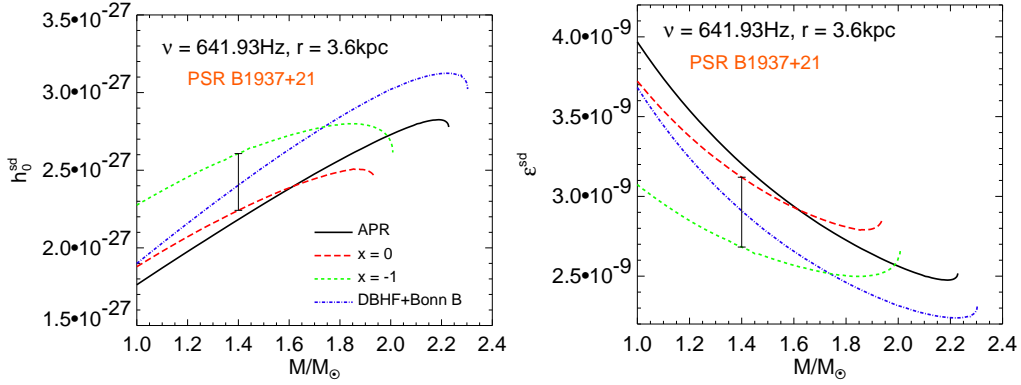


Figure 23: (Color online) Gravitational wave strain amplitude  $h_0^{sd}$  (left panel) and ellipticity (right panel), deduced from the spin-down rate of PSR B1937+21. See text for details.

past [108, 128]. These calculations have provided estimates for the gravitational wave strain amplitude of selected pulsars for which the spin-down rates are known, and also upper bounds for their ellipticities using the quadrupole model [108]. However, such calculations simply used the “fiducial” value of  $10^{45} \text{ g cm}^2$  for the moment of inertia  $I_{zz}$  in all estimates. On the other hand, the neutron star moment of inertia is sensitive to the details of the EOS of stellar matter, and especially to the density dependence of the nuclear symmetry energy [60]. Moreover,  $I_{zz}$  increases with increasing rotational frequency (see, e.g. Fig. 15) and the differences with the static values of the moment of inertia could be significant, particularly for rapidly rotating neutron stars.

The gravitational wave strain amplitude of PSR B1937+21 is shown in Fig. 23 (left panel). Because the MDI EOS is constrained by available nuclear laboratory data, our results with the  $x = 0$  and  $x = -1$  EOSs allowed us to place a rather conservative *upper* limit on the gravitational waves to be expected from this pulsar, provided the *only* mechanism accounting for its spin-down rate is gravitational radiation. Under these circumstances, the upper limit of the strain amplitude,  $h_0^{sd}$ , for neutron star models of  $1.4 M_\odot$  is in the range  $h_0^{sd} = [2.24 - 2.61] \times 10^{-27}$ . Similarly, we have constrained the upper limit of the ellipticity of PSR B1937+21 to be in the range  $\epsilon^{sd} = [2.68 - 3.12] \times 10^{-9}$  (Fig. 23, right panel).

## 8 Summary and outlook

In this chapter we have summarized our recent studies on properties of (rapidly) rotating neutron stars and the gravitational waves expected from deformed pulsars using several nuclear EOSs constrained partially by terrestrial laboratory experiments. In particular, the latest heavy-ion reaction experiments have constrained partially the density dependence of the nuclear symmetry energy and thus the EOS of neutron-rich nuclear matter. These limits, while being incomplete and still suffer from some remaining uncertainties, can already provide some useful information about the possible stable configurations of (rapidly) rotating neutron stars and the gravitational radiation expected from them. Specifically, we have studied properties of (rapidly) rotating neutron stars employing four nucleonic EOSs and find that the rapid rotation affects the neutron star structure significantly. It increases the

maximum possible mass up to  $\sim 17\%$  and increases/decreases the equatorial/polar radius by several kilometers. The neutron star moment of inertia has been studied for both slowly and rapidly rotating models within a well established formalism. We found that the moment of inertia of PSR J0737-3039A is limited in the range of  $I = (1.30 - 1.63) \times 10^{45} (g \text{ cm}^2)$ . The fractional momenta of inertia  $\Delta I/I$  of the neutron star crust are also constrained. It is also found that the moment of inertia increases with rotational frequency at a rate strongly depending upon the EOS used. Additionally, rotation reduces central density and proton fraction in the neutron star core, and depending on the exact stellar mass and rotational frequency could effectively close the fast cooling channel in millisecond pulsars. This circumstance may have important consequences for both the interpretation of cooling data and the thermal evolution modelling.

We have reported predictions on the upper limit of the strain amplitude of the gravitational waves to be expected from elliptically deformed pulsars at frequencies  $< 300Hz$ . Our results are intended to provide guidance to the ground-based gravitational wave observatories. By applying an EOS with symmetry energy constrained by recent nuclear laboratory data, we obtained an upper limit on the gravitational-wave signal to be expected from several pulsars. Depending on details of the EOS, for several millisecond pulsars  $0.18kpc$  to  $0.35Kpc$  from Earth, the *maximal*  $h_0$  is found to be in the range of  $\sim [0.4 - 1.5] \times 10^{-24}$ . Finally, from the spin-down rate of PSR B1937+21 we have deduced the upper limit of the strain amplitude,  $h_0^{sd}$ , for neutron star models of  $1.4M_\odot$  to be in the range  $h_0^{sd} = [2.24 - 2.61] \times 10^{-27}$ . We have also constrained the upper limit of the ellipticity of PSR B1937+21 to be in the range  $\epsilon^{sd} = [2.68 - 3.12] \times 10^{-9}$ . These predictions set the first direct nuclear constraints on the gravitational waves from elliptically deformed pulsars.

Looking forward, new experiments in terrestrial nuclear laboratories are expected to improve our understanding about the EOS of dense neutron-rich nuclear matter dramatically in the next few years. The EOS of neutron-rich matter will be better constrained in a wide density range. Most of the studies presented in this review will then be further refined. Conversely, rapid progress in astrophysical observations of neutron stars and gravitational waves surely will also help us better understand the EOS of neutron-rich matter, and thus stimulate the progress in nuclear physics. Eventually, the ultimate goal of understanding thoroughly all mysteries of pulsars can only be realized by utilizing the progress made in both nuclear physics and astrophysics.

## Acknowledgements

We thank Aaron Worley for his collaboration on some of the work reported here. This work is supported in part by the US National Science Foundation under Grants No. PHY0757839, the Research Corporation under Award No. 7123 and the Texas Coordinating Board of Higher Education Grant No.003565-0004-2007.

## References

- [1] N. K. Glendenning, *Compact Stars, Nuclear Physics, Particle Physics, and General Relativity* (New York: Springer-Verlag) (2000).
- [2] M. Bejger, P. Haensel, and J. L. Zdunik, *Astron. and Astrophys.* **464**, L49 (2006).
- [3] D. C. Backer, S. R. Kulkarni and C. Heiles et al., *Nature* **300**, 615 (1982).
- [4] F. Weber, *Pulsars as Astrophysical Laboratories for Nuclear and Particle Physics* (Bristol, Great Britan: IOP Publishing) (1999).
- [5] J. W. T. Hessels, S. M. Ransom, I. H. Stairs, P. C. C. Freire, V. M. Kaspi and F. Camilo, *Science* **311**, 1901 (2006).
- [6] P. Kaaret, J. Prieskorn, J. J. M. in't Zand et al., *Astrophys. J.* **657**, L97 (2007).
- [7] F. Weber and R. Negreiros, arXiv:0911.5164 [astro-ph.SR]
- [8] P. Danielewicz, R. Lacey and W. G. Lynch, *Science* **298**, 1592 (2002).
- [9] J. M. Lattimer and M. Prakash, *Science* **304**, 536 (2004).
- [10] A. W. Steiner, M. Prakash, J. M. Lattimer and P. J. Ellis, *Phys. Rept.* **411**, 325 (2004).
- [11] P. G. Krastev and F. Sammarruca, *Phys. Rev. C* **74**, 025808 (2006).
- [12] B. -A. Li, C. M. Ko and Z. -Z. Ren, *Phys. Rev. Lett.* **78**, 1644 (1997).
- [13] B. -A. Li, *Phys. Rev. Lett.* **85**, 4221 (2000).
- [14] B. -A. Li, *Phys. Rev. Lett.* **88**, 192701 (2002).
- [15] B. -A. Li, C. M. Ko and W. Bauer, *Int. J. Mod. Phys. E* **7**, 147 (1998).
- [16] B.-A. Li, L.-W. Chen and C.M. Ko, *Phys. Rep.* **464**, 113 (2008).
- [17] B. -A. Li and W. Udo Schroeder, *Isospin Physics in Heavy-Ion Collisions at Intermediate Energies* (New York: Nova Science) (2001).
- [18] V. Baran, M. Colonna, V. Greco and M. Di Toro, *Phys. Rept.* **410**, 335 (2005).
- [19] M. B. Tsang et al., *Phys. Rev. Lett.* **92**, 062701 (2004).
- [20] M. B. Tsang et al., *Phys. Rev. Lett.* **86**, 5023 (2001).
- [21] L. Shi and P. Danielewicz, *Phys. Rev. C* **68**, 064604 (2003).
- [22] L. W. Chen, C. M. Ko and B. -A. Li, *Phys. Rev. Lett.* **94**, 032701 (2005).
- [23] A. W. Steiner and B. -A. Li, *Phys. Rev. C* **72**, 041601 (2005).
- [24] B. -A. Li and L. -W. Chen, *Phys. Rev. C* **72**, 064611 (2005).



- 
- [25] M. B. Tsang et al., *Phys. Rev. Lett.* **102** (2009) 122701.
- [26] C. J. Horowitz and J. Piekarewicz, *Phys. Rev. Lett.* **86**, 5647 (2000).
- [27] C. J. Horowitz and J. Piekarewicz, *Phys. Rev. C* **66**, 055803 (2002).
- [28] B. G. Todd-Rutel and J. Piekarewicz, *Phys. Rev. Lett.* **95**, 122501 (2005).
- [29] M. Centelles et al., *Phys. Rev. Lett.* **102**, 122502 (2009).
- [30] P. Danielewicz and J. Lee, *Nucl. Phys. A* **818**, 36 (2009).
- [31] L. W. Chen, C. M. Ko, B. -A. Li and G. C. Yong, *Frontiers of Physics in China* **2**, 327 (2007).
- [32] Z. G. Xiao, B.A. Li, L.W. Chen, G.C. Yong and M. Zhang, *Phys. Rev. Lett.* **102**, 062502 (2009).
- [33] W. Reisdorf et al., *Nucl. Phys. A* **781**, 459 (2007).
- [34] M. Prakash, J. M. Lattimer, R. F. Sawyer and R. R. Volkas, *Ann. Rev. Nucl. Part. Sci.* **51**, 295 (2001).
- [35] J. M. Lattimer and M. Prakash, *Phys. Rept.* **333**, 121 (2000).
- [36] H. Heiselberg and M. Hjorth-Jensen, *Phys. Rept.* **328**, 237 (2000).
- [37] H. Heiselberg and V. Pandharipande, *Ann. Rev. Nucl. Part. Sci.* **50**, 481 (2000).
- [38] D. G. Yakovlev and C. J. Pethick, *Ann. Rev. Astron. Astrophys.* **42**, 169 (2004).
- [39] J. B. Hartle, *Astrophys. J.* **150**, 1005 (1967).
- [40] J. B. Hartle and K. S. Thorne, *Astrophys. J.* **153**, 807 (1968).
- [41] J. L. Friedman, L. Parker and J. R. Ipser, *Astrophys. J.* **304**, 115 (1986).
- [42] I. Bombaci, A. V. Thampan and B. Datta, *Astrophys. J.* **541**, L71 (2000).
- [43] J. M. Lattimer, M. Prakash, D. Masak, and A. Yahil, *Astrophys. J.* **355**, 241 (1990).
- [44] H. Komatsu, Y. Eriguchi and I. Hachisu, I., *Mon. Not. R. Astr. Soc.* **237**, 355 (1989).
- [45] G. B. Cook, S. L. Shapiro and S. A. Teukolsky, *Astrophys. J.* **424**, 823 (1994).
- [46] N. Stergioulas and J. L. Friedman, *Astrophys. J.* **444**, 306 (1994).
- [47] N. Stergioulas and J. L. Friedman, *Astrophys. J.* **492**, 301 (1997).
- [48] S. Bonazzola, E. Gourgoulhon and J. -A. Marck, J.-A., *Phys. Rev. D* **58**, 104020 (1998).
- [49] S. Bonazzola, E. Gourgoulhon, E. Salgado and J. -AMarck, *Astron. and Astrophys.* **278**, 421 (1993).

- 
- [50] M. Ansorg, A. Kleinwächter, and R. Meinel, *Astron. and Astrophys.* **381**, L49 (2002).
- [51] N. Stergioulas, *Living Rev. Rel.* **6**, 3 (2003).
- [52] A. Einstein, *Über Gravitationswellen. Sitzungsberichte der Preussischen Akademie der Wissenschaften zu Berlin*, 154 - 167 (1918).
- [53] J. M. Weisberg and J. H. Taylor, *Relativistic Binary Pulsar B1913+16: Thirty Years of Observations and Analysis, in Binary Radio Pulsars*, ASP Conference Series, Vol. 328, Proceedings of the conference held 11-17 January, 2004, Aspen, Colorado, USA. Edited by F.A. Rasio and I.H. Stairs. San Francisco: Astronomical Society of the Pacific, p.25 (2005).
- [54] B. -A. Li and A. W. Steiner, *Phys. Lett. B* **642**, 436 (2005).
- [55] P. G. Krastev and B. -A. Li, *Phys. Rev. C* **76**, 055804 (2007).
- [56] J. Xu, L. W. Chen, B. -A. Li, and H. R. Ma, *Phys. Rev. C* **79**, 035802 (2009); *ApJ* **697**, 1549 (2009).
- [57] D. H. Wen, B. A. Li and P. G. Krastev, *Phys. Rev. C*, **80**, 025801 (2009).
- [58] W. G. Newton and B. -A. Li, arXiv:0908.1731, *Phys. Rev. C* **80**, 065809 (2009).
- [59] P. G. Krastev, B.-A. Li, and A. Worley, *Astrophys. J.* **676**, 11701177 (2008).
- [60] A. Worley, P. G. Krastev, and B.-A. Li, *Astrophys. J.* bf 685, 390 (2008).
- [61] Plamen G. Krastev, Bao-An Li, and Aaron Worley, *Phys. Lett. B* **668**, 1 (2008).
- [62] J. M. Lattimer and M. Prakash, *Phys. Rept.* **442**, 109 (2007).
- [63] G. F. Bertsch and S. Das Gupta, *Phys. Rept.* **160**, 189 (1988).
- [64] B. -A. Li, C. B. Das, S. D. Gupta and C. Gale, *Phys. Rev. C* **69**, 011603 (R) (2004); *Nucl. Phys. A* **735**, 563 (2004).
- [65] C. B. Das, S. D. Gupta, C. Gale and B. -A. Li, B.-A., *Phys. Rev., C* **67**, 034611 (2002).
- [66] R. B. Wiringa, *Phys. Rev. C* **38**, 2967 (1988).
- [67] D. H. Wen, B. A. Li and L. W. Chen, *Phys. Rev. Lett.* **103**, 211102 (2009) [arXiv:0908.1922 [nucl-th]].
- [68] J. Piekraewicz, *Phys. Rev. C* **76**, 064310 (2007).
- [69] M. Prakash, T. L. Ainsworth and J. M. Lattimer, *Phys. Rev. Lett.* **61**, 2518 (1988).
- [70] H. Muller and B. Serot, *Phys. Rev. C* **52**, 2072 (1995).
- [71] B. -A. Li and C. M. Ko, *Nucl. Phys. A* **618**, 498 (1997).
- [72] B. -A. Li, G. C. Yong and W. Zuo, *Phys. Rev. C* **71**, 014608 (2005).

- 
- [73] M. Kutschera, *Phys. Lett. B* **340**, 1 (1994); *Z. Phys. A* **348**, 263 (1994); *Phys. Lett. B* **223**, 11 (1989); *Phys. Rev. C* **47**, 1077 (1993).
- [74] M. Kutschera and J. Niemiec, *Phys. Rev. C* **62**, 025802 (2000).
- [75] V. R. Pandharipande and V. K. Garde, *Phys. Lett. B* **39**, 608 (1972).
- [76] R. B. Wiringa, V. Fiks and A. Fabrocini, *Phys. Rev. C* **38**, 1010 (1988).
- [77] E. Chabanat et al., *Nucl. Phys. A* **627**, 710 (1997); *ibid* **635**, 231 (1998).
- [78] D. T. Khoa, W. Von Oertzen and A. A. Ogloblin, *Nucl. Phys. A* **602**, 98 (1996).
- [79] D. N. Basu, P. R. Chowdhury and C. Samanta, *Acta Phys. Polon. B* **37**, 2869 (2006); D. N. Basu and T. Mukhopadhyay, *ibid*, B **38**, 169 (2007); T. Mukhopadhyay and D. N. Basu, *ibid*, B **38**, 3225 (2007).
- [80] J. R. Stone, J. C. Miller, R. Koncewicz, P. D. Stevenson and M. R. Strayer, *Phys. Rev. C* **68**, 034324 (2003).
- [81] C. Xu and B. A. Li, arXiv:0910.4803.
- [82] A. Akmal, V. R. Pandharipande and D. G. Ravenhall, *Phys. Rev. C* **58**, 1804 (1998).
- [83] F. Sammarruca and P. Liu, arXiv:0806.1936 [nucl-th].
- [84] D. Alonso and F. Sammarruca, *Phys. Rev. C* **67**, 054301 (2003).
- [85] R. Machleidt, *Adv. Nucl. Phys.* **19**, 189 (1989).
- [86] K. S. Thorne, in: *Proc. Int. School of Phys. "Enrico Fermi"*, Course 35, High Energy Astrophysics, ed. by L. Gratton (New York: Academic Press) (1966).
- [87] R. C. Tolman, *Phys. Rev.* **55**, 364 (1939).
- [88] J. R. Oppenheimer and G. M. Volkoff, *Phys. Rev.* **55**, 374 (1939).
- [89] R. Ouyed, *Astron. and Astrophys.* **382**, 939 (2002).
- [90] C. J. Pethick, D. G. Ravenhall and C. P. Lorenz, *Nucl. Phys. A* **584**, 675 (1995).
- [91] P. Haensel and B. Pichon, *Astron. Astrophys.* **283**, 313 (1994).
- [92] J. L. Friedman, L. Parker and J. R. Ipser, *Nature* **312**, 255 (1984).
- [93] J. L. Friedman, J. R. Ipser and L. Parker, *Phys. Rev. Lett.* **62**, 3015 (1989).
- [94] P. Haensel and J. L. Zdunik, *Nature* **340**, 617 (1989).
- [95] F. Ozel, *Nature*, 441, 1115 (2006).
- [96] N. Stergioulas, *Doctoral Dissertation*, The University of Wisconsin-Milwaukee (1996).

- 
- [97] M. Burgay, N. D'Amico, A. Possenti, R. N. Manchester, A. G. Lyne, B. C. Joshi, M. A. McLaughlin, M. Kramer, J. M. Sarkissian, F. Camilo, V. Kalogera, C. Kim and D. R. Lorimer, *Nature* **426**, 531 (2003).
- [98] M. Bejger, T. Bulik and P. Haensel, *Mon. Not. Roy. Astron. Soc.* **364**, 635 (2005).
- [99] I. A. Morrison, T. W. Baumgarte, S. L. Shapiro and V. R. Pandharipande, *Astrophys. J.* **617**, L135 (2004).
- [100] J. M. Lattimer and B. F. Schutz, *Astrophys. J.* **629**, 979 (2005).
- [101] B. Link, R. I. Epstein and J. M. Lattimer, *Phys. Rev. Lett.* **83**, 3362 (1999).
- [102] S. Kubis, *Phys. Rev. C* **76**, 025801 (2007).
- [103] M. Baldo, G. F. Burgio and H. -J. Schulze, *Phys. Rev. C* **61**, 055801 (2000).
- [104] M. Prakash, M. Prakash, J. M. Lattimer, and C. J. Pethick, *Astrophys. J. Lett.* **390**, L77 (1992).
- [105] D. Page, U. Geppert and F. Weber, *Nucl. Phys. A* **777**, 497 (2005).
- [106] M. Maggiore, *Nature* **447**, 651 (2007).
- [107] E. E. Flanagan and S. A. Hughes, *New J. Phys.* **7**, 204 (2005).
- [108] B. Abbott *et al.* [LIGO Scientific Collaboration], *Phys. Rev. Lett.* **94**, 181103 (2005); *Phys. Rev. D* **76**, 042001 (2007).
- [109] F. Acernese *et al.*, *Class. Quant. Grav.* **24**, S491 (2007).
- [110] P. Jaranowski, A. Krolak and B. F. Schutz, *Phys. Rev. D* **58**, 063001 (1998).
- [111] V. R. Padharipande, D. Pines, and R. A. Smith, *Astrophys. J.* **208**, 550–566 (1976).
- [112] M. Zimmermann and E. Szedenis, *Phys. Rev. D* **20**, 351 (1979).
- [113] M. Zimmermann, *Phys. Rev. D* **21**, 891 (1980).
- [114] S. Bonazzola and E. Gourgoulhon, *Astron. Astrophys.* **312**, 675 (1996).
- [115] R. V. Wagoner, *Astrophys. J.* **278**, 345 (1984).
- [116] B. F. Schutz, in *Mathematics of Gravitation. Part II: Gravitational Wave Detection*, edited by A. Królak (Banach Center, Warsaw, 1997), Vol. 41, Pt. II, pp. 1117.
- [117] N. Andersson, *Astrophys. J.* **502**, 708 (1998).
- [118] F. Acernese *et al.*, *Class. Quant. Grav.* **22**, 869 (2005).
- [119] T. Creighton, *Class. Quant. Grav.* **20**, 853 (2003).
- [120] B. Haskell, N. Andersson, D. I. Jones, and L. Samuelsson, *Phys. Rev. Lett.* **99**, 231101 (2007).

- 
- [121] B. J. Owen, *Phys. Rev. Lett.* **95**, 211101 (2005).
- [122] C. J. Horowitz and Kai Kadau, *Phys. Rev. Lett.* **102**, 91102 (2009).
- [123] B. Haskell, D. I. Jones, and N. Andersson, *Mon. Not. R. Astron. Soc.* **373**, 1423 (2006).
- [124] M. Bailes et al., *Astrophys. J.* **481**,386 (1997).
- [125] A. W. Hotan, M. Bailes, and S. M. Ord, *Mon. Not. R. Astron. Soc.* **369**, 1502 (2006).
- [126] W. van Straten, M. Bailes, M. C. Britton, S. R. Kulkarni, S. B. Anderson, R. N. Manchester, and J. Sarkissian, *Nature* **412**, 158 (2001).
- [127] W. Laarakkers and E. Poisson, *Astrophys. J.* **512**, 282-287 (1999).
- [128] B. Abbott *et al.* [LIGO Scientific Collaboration] *Phys. Rev. D* **76**, 042001 (2007).
- [129] B. Abbott *et al.* [The LIGO Scientific Collaboration], *Astrophys. J.* **683**, L45 (2008) [Erratum-*ibid.* **706**, L203 (2009)] [arXiv:0805.4758 [astro-ph]].
- [130] G. Cusumano, W. Hermsen, M. Kramer, L. Kuiper, O. Lohmer, T. Mineo, L. Nicastro, and B. W. Stappers, *Nucl. Phys. Proc. Suppl.* **132**, 596 (2004).
- [131] R. N. Manchester, G. B. Hobbs, A. Teoh, and M. Hobbs, *Astron. J.* **129**, 1993 (2005).